國 立 交 通 大 學

電信工程研究所

碩 士 論 文

階層式基地台合作技術之效能評估

Performance Evaluation of Hierarchical Base Station Cooperation Techniques

研究生：蔣宗廷

指導教授：王蒞君 教授

中 華 民 國 一百 年 九 月

階層式基地台合作技術之效能評估

Performance Evaluation of Hierarchical Base Station Cooperation Techniques

研 究 生：蔣宗廷　　Student：Tsung-Ting Chiang

指導教授：王蒞君　　Advisor：Li-Chun Wang

國 立 交 通 大 學

電信工程研究所

碩 士 論 文

A Thesis

Submitted to Institute of Communications Engineering

College of Electrical and Computer Engineering

National Chiao Tung University

in partial Fulfillment of the Requirements

for the Degree of

Master of Science

In

Communication Engineering

September 2011

Hsinchu, Taiwan, Republic of China

中華民國 一百 年 九 月

階層式基地台合作技術之效能評估

學生：蔣宗廷　　指導教授：王蒞君　教授

國立交通大學

電機學院電信工程研究所

摘要

在本篇論文中，我們在第三代合作夥伴計劃-長期演進技術的環境下，介紹多重輸入多重輸出及階層式基地台合作之模擬平台的建構方法，並且符合目前第三代合作夥伴計劃的模擬結果。除此之外，我們同時去分析頻譜使用效率及能源使用效率。據我們所知，目前文獻上並沒有針對階層式基地台合作，同時評估其頻譜使用效率及能源使用效率的系統。我們發現，不同的系統在頻譜使用效率及能源使用效率上會有所取捨。在階層式基地台合作技術下，使用單一細胞識別可以獲得較佳的能源使用效率，然而，使用多細胞識別則可以獲得較好的頻譜使用效率。

Abstract

In this thesis, we discuss the methodology for evaluating the multi-input multi-output (MIMO) systems in the 3^{rd} Generation Partnership Project (3GPP) Long-Term Evolution-Advanced (LTE-A) environment, and give consistent simulation results with those from the other partners in 3GPP. Moreover, we evaluate the hierarchical base station cooperation (HBSC) systems and give some guidelines for designing the hierarchical cell architectures. Both spectral efficiency ($bits/s/Hz$) and energy efficiency ($bits/Joule$) are investigated in our systems. To the best of our knowledge, research papers considering both spectral efficiency and energy efficiency for the HBSC systems in the LTE-A environment are rarely seen in the literature. We find some interesting guildline to evaluate the tradeoffs between spectral efficiency and energy efficiency in the HBSC systems. Compared with the single cell ID HBSC system, we obtain a higher spectral efficiency but a lower energy efficiency by adopting the HBSC system with multiple cell IDs.

Acknowledgments

I especially would like to thank professor Li-Chun Wang who gave me not only many valuable suggestions in the research during these two years but also lots of encouragements. I would not finish this work without his guidance and comments.

In addition, I am deeply grateful to my laboratory mates, Dr. Meng-Lin Ku, Dr. Chu-Jung Yeh, Ang-Hsun, Ssu-Han, Yeh-Teng, Yu-Jung, Kai-Ping, Chien-Cheng, Wei-Ping, and junior laboratory mates in Mobile Communications and Cloud Computing Laboratory at the Institute of Communications Engineering in National Chiao-Tung University. They always provide me much assistance and share much happiness with me. Special thanks should go to Yi-Ting Lee who gives me great encouragement and cares for me all of my life.

Finally, I am indebted to my parents and younger sister for their kindliness and endless supports.

Contents

Abstract **I**

Acknowledgements **II**

List of Tables **VI**

List of Figures **VII**

1 Introduction **1**

1.1 Problem and Solution 3

1.2 Thesis Outline 4

2 Background **6**

2.1 Literature Survey 6

2.2 3GPP LTE-A Systems 7

2.3 LTE-A System-Level Simulator 9

3 System Models **11**

3.1 Channel Model 11

3.1.1 Spatial Channel Model 11

3.1.2 Radio Environments 14

3.2 Cellular MIMO Systems 16

3.3 Hierarchical Base Station Cooperation Systems 16

3.3.1 Cooperation with Single Cell ID 17

3.3.2 Cooperation with Multiple Cell IDs . . . 19
3.4 Power Consumption Model . . . 22

4 MIMO Physical Layer Simulation Platform 24
4.1 Codebook-based Precoder . . . 25
4.2 Receiver Structure . . . 30
4.3 Rank Adaptation and SU/MU-MIMO Switching . . . 32
4.4 Proportional Fair Scheduling . . . 33

5 Hierarchical Base Station Cooperation Simulation Platform 35
5.1 RRH Nodes Selection . . . 35
5.1.1 Cooperation with Single Cell ID . . . 35
5.1.2 Cooperation with Multiple Cell IDs . . . 36
5.2 Transmit Signal Model . . . 37
5.2.1 Cooperation with Single Cell ID . . . 37
5.2.2 Cooperation with Multiple Cell IDs . . . 38
5.3 Receiver Structure . . . 41
5.3.1 Cooperation with Single Cell ID . . . 41
5.3.2 Cooperation with Multiple Cell IDs . . . 42

6 Numerical Results 44
6.1 MIMO in LTE-A Systems . . . 44
6.2 Hierarchical Base Station Cooperation . . . 47
6.2.1 Cooperation with Single Cell ID . . . 47
6.2.2 Cooperation with Multiple Cell IDs . . . 51
6.3 Summary . . . 56

7 Conclusions and Future Research 64
7.1 Conclusions . . . 64
7.2 Future Research . . . 65

Bibliography **66**

Vita **70**

List of Tables

2.1 **Comparison of Our Work and Other Literatures** 7

4.1 **Release 9 Two Antenna Ports Codebook** 27
4.2 **Release 9 Four Antenna Ports Codebook** 28

6.1 **Simulation Parameters for MIMO systems** 59
6.2 **Performance Evaluation Comparison** 60
6.3 **Simulation Parameters for RRH Nodes** 61
6.4 **Total System Consumed Power per Sector in HBSC-S Systems** 62
6.5 **Total System Consumed Power per Sector in HBSC-M Systems** 62
6.6 **Comparison between Energy Efficiency and Spectral Efficiency (d = 0.6R)** 63

List of Figures

1.1 Conventional MIMO systems. 2
1.2 Network MIMO systems. 3

2.1 Frame structure in the downlink and the uplink. 10

3.1 SCM parameters of the user and base station. 13
3.2 Horizontal antenna pattern for the 3GPP macro-cell. 15
3.3 Cell architecture of MIMO systems. 17
3.4 Cell architecture of the HBSC-S systesm. 18
3.5 Cell architecture of the HBSC-M systesm. 20

4.1 Flow chart for the physical layer simulator. 26

5.1 Non-cooperation transmission mode in the hierarchical system. 39

6.1 Spectral efficiency for 2x2 SU-MIMO with different codebook selection mechanisms. 45
6.2 MIMO downlink normalized user throughput in LTE-A systems. . . . 46
6.3 5% cell-edge spectral efficiency of the HBSC-S systems without ICI. . 48
6.4 5% cell-edge spectral efficiency of the HBSC-S systems. 50
6.5 Cell-average spectral efficiency of the HBSC-S systems. 50
6.6 Energy efficiency of the the HBSC-S systems. 52
6.7 5% cell-edge spectral efficiency of the HBSC-M systems. 54
6.8 Cell-average spectral efficiency of the HBSC-M systems. 54

6.9 Energy efficiency of the HBSC-M systems. 55
6.10 Comparison between energy efficiency and spectral efficiency , $d = 0.6R$. 57
6.11 Power consumption per sector of HBSC systems for targeting at 2.40 bits/s/Hz. 57


E S A
1896

CHAPTER 1

Introduction

With the rapid growth in the demand for high data rate , the multi-input multi-output (MIMO) antenna system technique is one of the key techniques that can be used to improve radio link throughput [1]. However, because of the inter-cell interference (ICI), the spectral efficiency of MIMO systems at the cell edge is significantly degraded. As shown in Fig. 1.1, if a user is located at the cell edge, it suffers severe inter-cell interference from the neighboring macro cell.

To mitigate the inter-cell interference resulted from the neighboring cells and to enhance the signal-to-interference-plus-noise (SINR) ratio, the concept of joint MIMO processing among cooperative multiple base stations (BSs), referred to network MIMO, has recently been proposed [2–6]. Fig. 1.2 illustrates the general idea of the network MIMO system. The cooperative BSs are connected by the high-speed backhaul (e.g. optical fiber). With the backhaul, some certain information, i.e. channel state information (CSI) and transmit data, can be interchanged via the backhaul. Hence, the cooperative BSs can jointly work MIMO processing just like a huge virtual-MIMO system. Advanced network MIMO techniques, such as switching between conventional MIMO systems and network MIMO [7], and the combining of frequency partition and network MIMO [8], have been proposed to further enhance the downlink throughput of the network MIMO systems.

The network MIMO technique has become a potential solution that can be

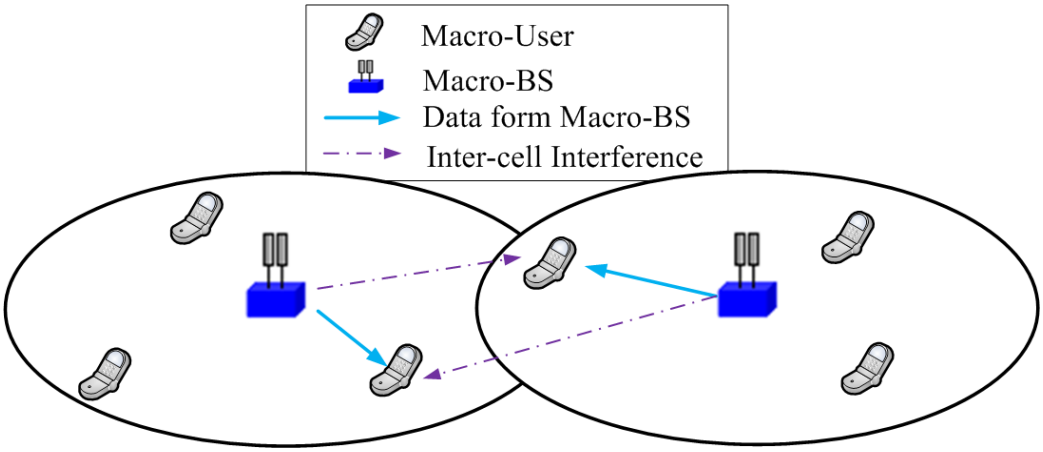

Figure 1.1: Conventional MIMO systems.

used to eliminate ICI in the next-generation wireless systems, such as the IEEE 802.16m Worldwide Interoperability for Microwave Access (WiMAX) standard and the Third Generation Partnership Project (3GPP) Long-Term Evolution-Advanced (LTE-A) standard. In IEEE 802.16m WiMAX, there are two scenarios for multi-BS processing (1) closed-loop marco diversity (CL-MD) and (2) collaborative MIMO (Co-MIMO) transmission. To apply CL-MD transmission, a single user is served jointly by multiple cooperative BSs. To apply the Co-MIMO transmission, several users are served jointly by multiple cooperative BSs [9]. A similar concept is proposed in the LTE-A standard, called coordinated multi-point (CoMP) transmission. There are three scenarios (1) coordinated scheduling/coordinated beamforming (CS/CB), (2) single-user (SU) joint processing (JP) (corresponding to CL-MD in WiMAX), and (3) multi-user (MU) JP (corresponding to Co-MIMO in WiMAX). CS/CB is another technique that several BSs are coordinated to schedule users and search the suitable beamforming matrix for each user [10–13]. The data is transmitted only from the single BS. These approaches are worse than the JP techniques but reduce the amount of exchanging data via the backhaul. Single-user-JP-CoMP is similar to

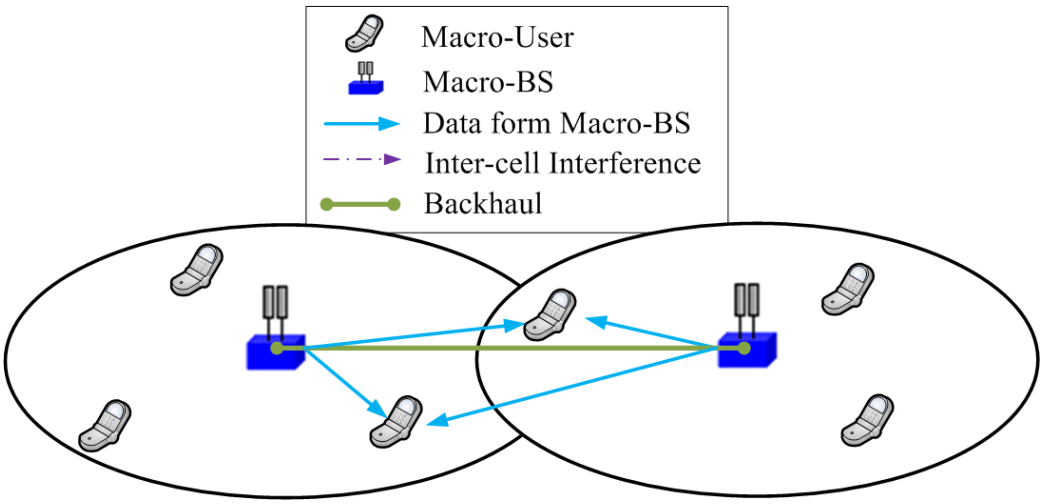

Figure 1.2: Network MIMO systems.

CL-MD where multiple BSs jointly serve a single user. Both multi-user-JP-CoMP and Co-MIMO transmissions allow multiple coordinated BSs to serve multiple users simultaneously with jointly designed precoding matrix.

1.1 Problem and Solution

Network MIMO is one of the potential techniques for a next-generation wireless system to eliminate ICI and enhance the cell-edge spectral efficiency. Generally, neighboring cells in a network MIMO system are linked by a high-speed backhaul to exchange users' information. Hence, several BSs can cooperate to provide joint MIMO signal processing. However, cooperating at the large-cell level (e.g. macro-cell) results in higher cost and more complex system design. This is because the distance between cooperative BSs is too long. The cost of the backhaul connection and the synchronization issues are crucial. In [14], it was shown that the performance of the network MIMO system degrades significantly when considering the large feedback

delay. Hence, we do not cooperate cells in a large area. On the contrast, we place some low power BSs, e.g. RRH nodes, at the edges of macro-cells and cooperate these nodes in a smaller area.

Moreover, we consider two different RRH types (1) RRH nodes that share the same cell ID with the corresponding macro-BS and, (2) RRH nodes for which each RRH node has an individual cell ID that is different from the corresponding macro-BS. These two types of RRH nodes result in a difference in performance. In (1), the macro-BS and the RRH nodes with the same cell ID are cooperated, and we refer to the system as **H**ierarchical **B**ase **S**tation **C**ooperation with the **S**ingle cell ID (HBSC-S). In (2), the macro-BS and the RRH nodes with the different cell IDs are cooperated, and we refer to the system as **H**ierarchical **B**ase **S**tation **C**ooperation with **M**ultiple cell IDs (HBSC-M). Generally, the HBSC-S system is simple but has lower spectral efficiency, whereas the HBSC-M system is complex but has higher spectral efficiency.

We evaluate both HBSC-S and HBSC-M systems as well as conventional MIMO systems in an LTE-A environment. The performance of the conventional MIMO system is demonstrated and compared with the existing results in 3GPP. Then, we analyze both spectral efficiency and energy efficiency of the cooperation systems, and illustrate the tradeoffs between spectral efficiency and energy efficiency.

1.2 Thesis Outline

The rest of this thesis is organized as follows. The background of our work is introduced in Chapter 2. The overall system models are described in Chapter 3. In Chapter 4, we disscuss the simulation methodology of MIMO systems in the LTE-A environment. Chapter 5 discusses the detailed HBSC system. Subsequently, numerical results are shown in Chapter 6. Finally, we conclude this thesis and discuss

potential future works in Chapter 7.

CHAPTER 2

Background

2.1 Literature Survey

Many researchers have investigated several cooperation schemes. In [3], they provided both the theoretic upper-bound and some practical schemes in the downlink cooperation systems. The upper bound was obtained by implementing the dirty paper coding (DPC). In [4], the singular value decomposition (SVD) based network MIMO scheme with various antenna number was investigated. They concluded that cooperating among several cells can bring the enormous gain in the spectral efficiency and showed that the capacity increases as the antenna number increases. In [6], the performance of cooperation among various cell number was discussed. The author concluded that the throughput can be improved if the number of cooperative cells or the number of sectors per cell increases. However, [3,4,6] only cooperated BSs at the large-cell level, and do not take into account of feedback accuracy. Moreover, they only considered the spectral efficiency rather then energy efficiency.

In [15], they illustrated the BS deployment strategies under cellular networks from the energy efficiency aspects. It placed some low-power nodes in the macro-cell to enhance the cell-edge throughput. Moreover, they introduce two concepts, i.e., the area power consumption and the area spectral efficiency. The area power consumption is used to estimate the total power consumption relative to the coverage

Table 2.1: **Comparison of Our Work and Other Literatures**

	Cooperation	**Hierarchical Cells**	**Spectral Efficiency Analysis**	**Energy Efficiency Analysis**	**LTE-A Environment**
[4]	√	×	√	×	×
[6]	√	×	√	×	×
[15]	×	√	×	√	×
[16]	√	×	×	√	×
Our Work	√	√	√	√	√

in Watts per square kilometers, and the area spectral efficiency is used to estimate the spectral efficiency relative to the coverage in bits per second per Hertz per square kilometers. The performance with the various number of low-power nodes was also investigated. However, they did not deal with the extra intra-cell interference caused by the low-power nodes. In [16], the author demonstrated the additional consumed power including signal processing power, backhaul power, and pilots power. They also consider the signalling overhead including pilots and CSI feedback. With the various cell sizes and cooperation sizes, the author indicated that cooperating more than three macro-cells is not energy-efficient. However, only one BS type, i.e., macro-cell, was considered. We compare our work with the above research in Table 2.1. We investigate both spectral efficiency and energy efficiency in our hierarchical cooperation systems. Moreover, we evaluate the systems in the LTE-A environment.

2.2 3GPP LTE-A Systems

The 3^{rd} Generation Partnership Project (3GPP) has adopted orthogonal frequency division multiple access (OFDMA) in the downlink and single carrier frequency division multiple access (SC-FDMA) in the uplink of LTE-A systems. The advantages

of using OFDMA in the downlink include not only overcoming the multipath problem, but also making use of the adaptive modulation and coding schemes (MCS). On the other hand, the advantage of using SC-FDMA is the ability to reduce the peak-to-average power ratio (PAPR).

To achieve the target downlink peak spectral efficiency of 30 bits/s/Hz and uplink peak spectral efficiency of 15 bits/s/Hz [17], many techniques have been suggested for the 3GPP LTE-A systems, including SU-MIMO, MU-MIMO, relaying techniques, carrier aggregation (CA), enhanced inter-cell interference coordination (eICIC), and CoMP. SU-MIMO is a common technique to improve radio link throughput in 3GPP LTE-A systems. It utilizes transmit diversity or multiple spatial layers to transmit the data to a single user equipment (UE). Several transmission modes are adopted, e.g. transmit diversity, open-loop spatial multiplexing, closed-loop spatial multiplexing, beamforming, etc. In MU-MIMO systems, the BS serves multiple users in the same time-frequency resource by making use of degrees of freedom (DoF) in the spatial domain. It enhances the cell-average spectral efficiency as compared to SU-MIMO systems. Relay nodes are connected with the BS wirelessly and help further serve the cell-edge users. CA is used to collect several discontinuous frequency bands and hence we can utilize a larger bandwidth up to 100 MHz. CoMP and eICIC are two techniques used to control the inter-cell interference, where the former uses the cooperation among certain BSs and the latter takes advantage of radio resource management (RRM).

In order to catch on the detailed time-frequency resource used in LTE-A systems, we need to understand the physical resource block (RB) defined in [18]. One radio frame with 10 milliseconds consists of 20 time slots. Each time slots can divided into N_{RB}^{UL} resource blocks (RBs) and N_{RB}^{DL} RBs for the uplink and downlink respectively. In the frequency domain, both the uplink RB and the downlink RB consist of N_{sc}^{RB} subcarriers. In the time domain, one uplink RB consists of N_{symb}^{UL} SC-FDMA

symbols and one downlink RB consists of N_{symb}^{DL} OFDM symbols. Hence, one uplink RB consists of $N_{sc}^{RB} \times N_{symb}^{UL}$ resource elements (REs) and one downlink RB consists of $N_{sc}^{RB} \times N_{symb}^{DL}$ REs. We show the frame structure in Fig. 2.1.

2.3 LTE-A System-Level Simulator

For the purpose of evaluating the performance and proposing practicable schemes under the LTE-A standard, it is necessary to build the LTE-A simulator. To our knowledge, many equipment vendors and some research centers have already constructed their own simulators, but rarely describe their simulation methodology. In [19] and [20], they built a LTE-A simulation platform but did not compare their results with LTE-A calibration results. We have shown the calibration results compared with [21–23] in our lab (Mobile Communication and Cloud Computing Lab, Institute of Communications Engineering, National Chiao-Tung University) [24]. By examining the two steps (step (1a) for wideband SINR and step (1c) for spectral efficiency) performance metrics defined in [22], our lab's work is consistent with other existing simulation calibration results.

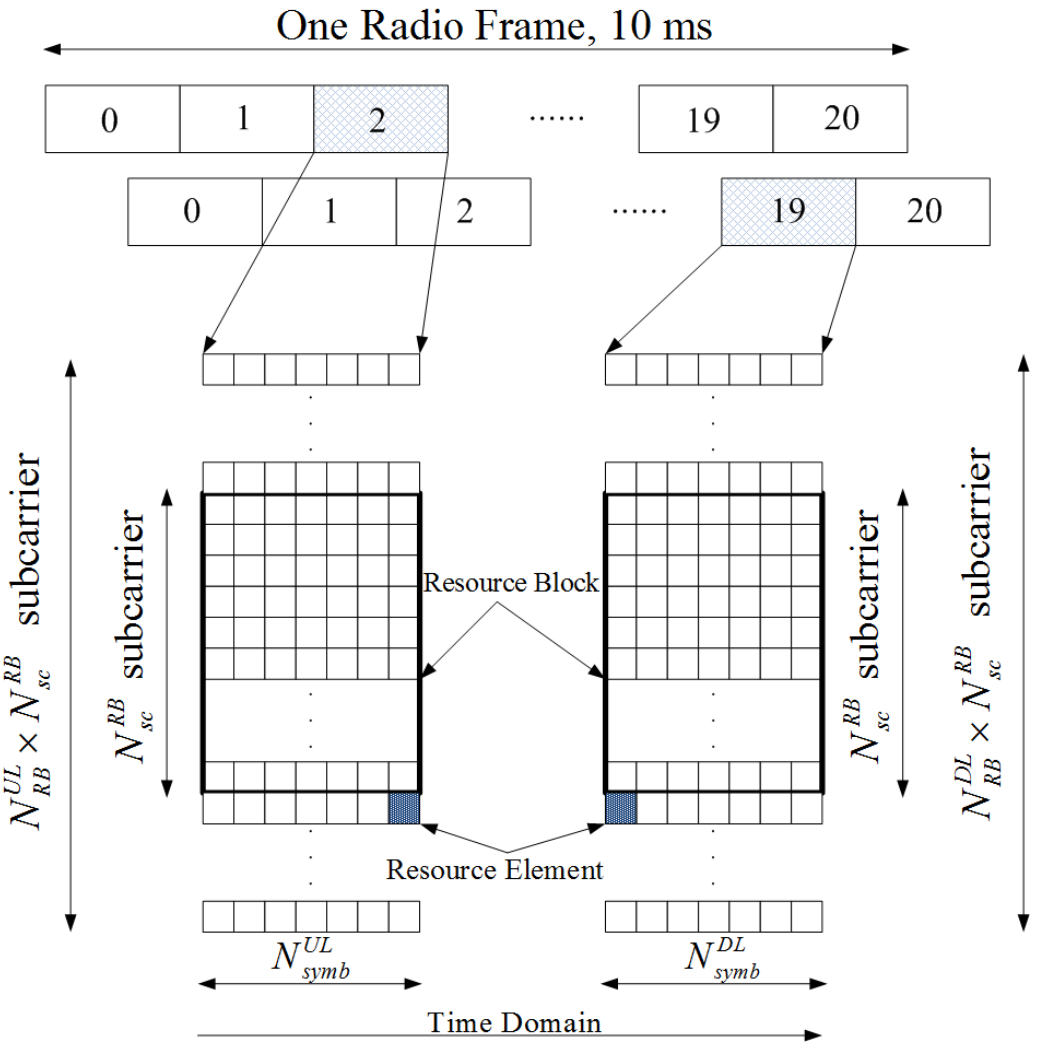

Figure 2.1: Frame structure in the downlink and the uplink.

CHAPTER 3

System Models

In this chapter, we introduce our system models in detail. Three cellular system models are described in the first three sections, i.e., cellular MIMO systems, hierarchical hierarchical BS cooperation with single cell ID (HBSC-S), and hierarchical BS cooperation with multiple cell IDs (HBSC-M). In the last section, we discuss the energy consumption issues and give reasonable models for each cellular system.

3.1 Channel Model

A suitable propagation channel model is important for numerical analysis. It models how the transmit signals propagate through the air space. Thus, we follow the channel model to characterize radio effects in the 3GPP LTE-A environment [22] and introduce each parameter in the following section.

3.1.1 Spatial Channel Model

The spatial channel model (SCM) is widely used in LTE-A systems simulation [25, 26]. In the early years, the International Telecommunication Union Radiocommunication Sector (ITU-R) channel model was developed for the International Mobile Telecommunications-2000 (IMT-2000) systems. However, the ITU-R channel model is not well-defined due to the renewed parameters, such as bandwidth, frequency

band. Moreover, the ITU-R model is not suitable for the MIMO systems since it does not model the spatial correlation between antennas. Hence, SCM has been developed to model the channel more correctly. As we know, SCM characterizes the spatial correlations as well as the multi-path fading. In the following, we discuss the formulations and parameters of SCM briefly.

The urban-macro scenario is adopted in our SCM simulations [22]. The macro-cell usually serves a large area, and hence the probability of experiencing a line-of-sight (LOS) environment tends to zero. Therefore, the LOS component can be neglected. Assume that there are N paths with each consisting of M subpaths in each link from the BS to the user. We introduce each parameter in Fig. 3.1:

θ_{BS} : the angle between the LOS and the BS array broadside.

θ_{User} : the angle between the LOS and the user array broadside.

$\delta_{n,AoD}$: the angle between the LOS and the n^{th} $(n = 0, 1, 2, ..., N-1)$ path.

$\delta_{n,AoA}$: the angle between the LOS and the n^{th} $(n = 0, 1, 2, ..., N-1)$ path.

$\Delta_{n,m,AoD}$: the offset of the m^{th} $(m = 0, 1, 2, ..., M-1)$ subpath within the n^{th} path relative to $\delta_{n,AoD}$.

$\Delta_{n,m,AoD}$: the offset of the m^{th} $(m = 0, 1, 2, ..., M-1)$ subpath within the n^{th} path relative to $\delta_{n,AoA}$.

θ_V : the angle between the user movement direction and the user array broadside.

$\theta_{n,m,AoA}$: $\theta_{n,m,AoA} = \theta_{User} + \delta_{n,AoA} + \Delta_{n,m,AoA}$.

$\theta_{n,m,AoD}$: $\theta_{n,m,AoA} = \theta_{BS} + \delta_{n,AoD} + \Delta_{n,m,AoD}$.

Assuming N_t transmit antennas at BS and N_r receive antennas at user, we can

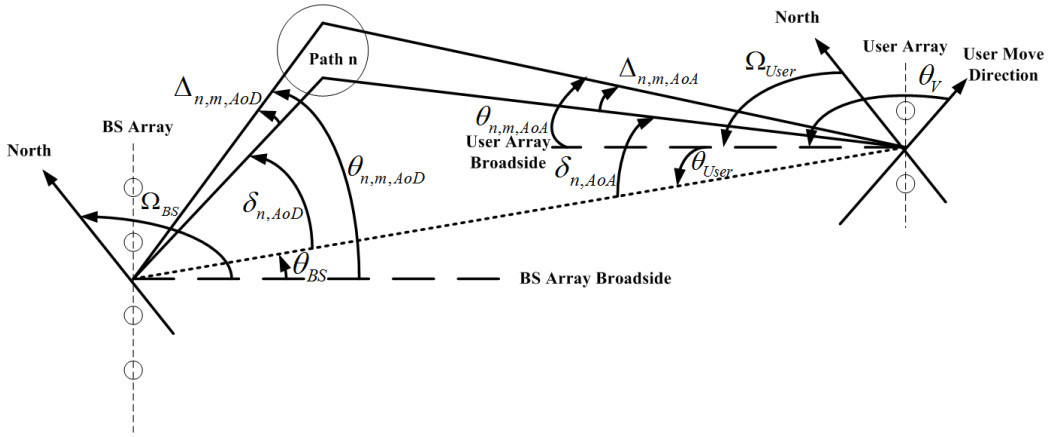

Figure 3.1: SCM parameters of the user and base station.

formulate the channel response matrix $\mathbf{h}^n(t) \in \mathcal{C}^{N_r \times N_t}$ as

$$\mathbf{h}^n(t) = \begin{bmatrix} h^{1,1,n}(t) & h^{1,2,n}(t) & \cdots & h^{1,N_t,n}(t) \\ h^{2,1,n}(t) & h^{2,2,n}(t) & \cdots & h^{2,N_t,n}(t) \\ \vdots & \vdots & \cdots & \vdots \\ h^{N_r,1,n}(t) & h^{N_r,2,n}(t) & \cdots & h^{N_r,N_t,n}(t) \end{bmatrix}. \tag{3.1}$$

Each element in $\mathbf{h}^n(t)$ can be written as :

$$h^{u,s,n}(t) = \sqrt{\frac{P_n}{M}} \sum_{m=1}^{M} \left(e^{jkd_s \sin(\theta_{n,m,AoD} + \psi_{n,m})} e^{jkd_u \sin(\theta_{n,m,AoA})} e^{jkV \cos(\theta_{n,m,AoA} - \theta_V)t} \right), \tag{3.2}$$

where P_n is the power of the n^{th} path, $\theta_{n,m,AoD}$ is the angle between the m^{th} subpath within the n^{th} path and the BS array broadside, $\theta_{n,m,AoA}$ is the angle between the m^{th} subpath within the n^{th} path and the user array broadside, M is the number of subpaths per path, k is the carrier wavelength in meters, d_s is the distance from the first antenna to the s^{th} antenna at the BS in meters, d_u is the distance from the first antenna to the u^{th} antenna at the user in meters, $\psi_{n,m}$ is the phase of the m^{th} subpath within the n^{th} path with uniform distribution in the interval $[0°, 360°]$, V is the user

speed, and θ_V is the angle between the user movement direction and the user array broadside.

Note that (3.1) is defined in the time domain. In order to apply the OFDM system, we must transform the time domain channel response into frequency domain. Let N_{FFT} denote the fast Fourier transform (FFT) size. The SCM for the k^{th} subcarrier in the frequency domain can be formulated as

$$\mathbf{H}^{SCM}(k) = \begin{bmatrix} H^{1,1}(k) & H^{1,2}(k) & \cdots & H^{1,N_t}(k) \\ h^{2,1}(k) & H^{2,2}(k) & \cdots & H^{2,N_t}(k) \\ \vdots & \vdots & \cdots & \vdots \\ H^{N_r,1}(k) & H^{N_r,2}(k) & \cdots & H^{N_r,N_t}(k) \end{bmatrix}, k = 1, 2, ..., N_{FFT} \ . \tag{3.3}$$

Each element of $\mathbf{H}(k)$ can be written as

$$H^{u,s}(k) = FFT\left[h^{u,s,1}(t), h^{u,s,1}(t), ..., h^{u,s,N}(t)\right] \ , \tag{3.4}$$

where $H^{u,s}(k)$ denotes the channel response coefficient from the s^{th} transmit antenna to the u^{th} receive antenna in the k^{th} subcarrier, FFT denotes the FFT function with size N_{FFT}, and $h^{u,s,n}(t)$ was shown in (3.2).

3.1.2 Radio Environments

Directional antenna pattern, path-loss model, and shadowing model are considered in our radio environment. A horizontal antenna pattern is defined for each fixed sector in 3GPP LTE-A systems [22]. It can be shown as

$$A^{dB}_{s,b,u}(\phi) = -\min\left[12\left(\frac{\phi_{s,b,u}}{\phi_{3dB}}\right)^2, A_m\right], \tag{3.5}$$

where $\phi_{s,b,u}$ is the angle between the beam direction of the s^{th} BS and the u^{th} user in the b^{th} sector, ϕ_{3dB} is 70 degrees, and A_m is 25 dB. Note that ϕ_{3dB} denotes the 3 dB power attenuation angle. Figure 3.2 shows the antenna pattern in simulation.

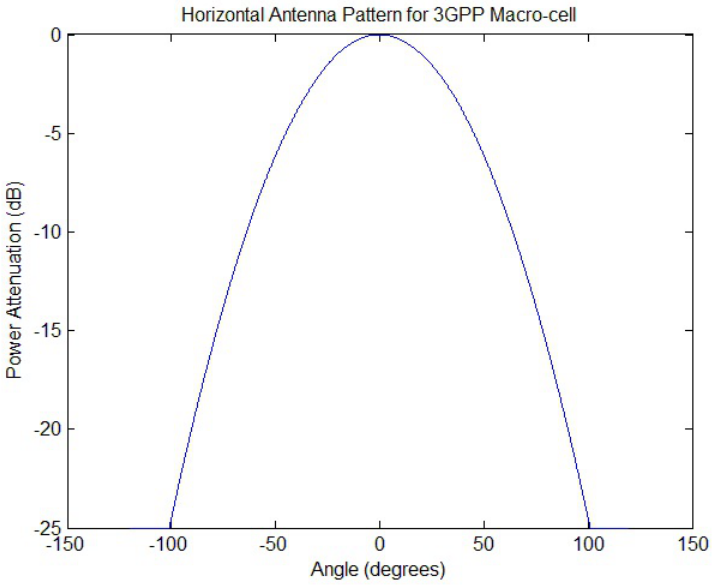

Figure 3.2: Horizontal antenna pattern for the 3GPP macro-cell.

Pathloss is the power attenuation when transmitting signals through the space. The pathloss model is usually represented as the difference between the transmit signal power and the receive signal power in decibels. The path-loss model has been defined for the macro-cell in [22] :

$$PL_{s,b,u}^{dB} = 128.1 + 37.6\log_{10}(d_{s,b,u}), \tag{3.6}$$

where $PL_{s,b,u}^{dB}$ is the power-loss term between the s^{th} BS and the u^{th} user in the b^{th} sector, and d is the distance from the s^{th} BS to the u^{th} user in the b^{th} sector in kilometers. The shadowing effect is caused by obstacles. It is modeled by the log-normal distribution with zero mean and 8 dB standard deviation.

For simplicity, we describe our following channel model in the single-carrier case. It can be extended to the multi-carrier case in the same way. Let $\mathbf{H}_{s,b,u} \in \mathcal{C}^{N_r \times N_t}$ denote the overall channel response including the spatial channel model and radio

effects. Thus, we can derive the overall complex baseband channel response as

$$\mathbf{H}_{s,b,u} = \mathbf{H}^{SCM}\sqrt{\eta_{s,b,u}A_{s,b,u}(PL_{s,b,u})^{-1}}\ , \tag{3.7}$$

where $\mathbf{H}_{s,b,u}$ is the channel response from the s^{th} BS to the u^{th} user in the b^{th} sector, $\mathbf{H}^{SCM} \in \mathcal{C}^{N_r \times N_t}$ is the SCM matrix shown in (3.3), $\eta_{s,b,u}$ is the log-normal distribution shadowing with zero mean and 8 dB standard deviation, $A_{s,b,u} = 10^{\left(A^{dB}_{s,b,u}/10\right)}$, and $PL_{s,b,u} = 10^{\left(PL^{dB}_{s,b,u}/10\right)}$.

3.2 Cellular MIMO Systems

The cellular system consists of 19 cell cites with hexagonal grid as shown in Fig. 3.3. Each hexagonal grid macro-cell is divided into three sectors, where each sector is equipped with directional antennas. Recall that there are N_t transmit antennas at each BS, N_r receive antennas at each user, and total N_u users in each sector. Denote $\mathbf{H}_{s,b,u} \in \mathcal{C}^{N_r \times N_t}$ as the channel matrix from the s^{th} BS to the u^{th} user in the b^{th} sector, $\mathbf{X}_{b,u}$ as the desired signal of the u^{th} user in the b^{th} sector, and $\mathbf{W}_{b,u}$ as the corresponding weighting matrix for the u^{th} user in the b^{th} sector, respectively. Generally, the receive signal can be modeled as follows

$$\mathbf{Y}_{b,u} = \underbrace{\mathbf{H}_{b,b,u}\mathbf{W}_{b,u}\mathbf{X}_{b,u}}_{\text{desired signal}} + \underbrace{\sum_{m \neq b}\mathbf{H}_{m,b,u}\mathbf{W}_{m,n}\mathbf{X}_{m,n}}_{\text{inter-cell interference}} + \mathbf{n}_{b,u}\ , \tag{3.8}$$

where $\mathbf{n_{b,u}} \in \mathcal{C}^{\mathbf{N_r \times 1}}$ is the additive white noise with $\sigma_n^2 = -174$ dBm/Hz power density.

3.3 Hierarchical Base Station Cooperation Systems

In this section, we discuss the models of HBSC systems. Several RRH nodes are fixed in each macro-cell and each RRH node is connected to the macro-BS by the backcaul

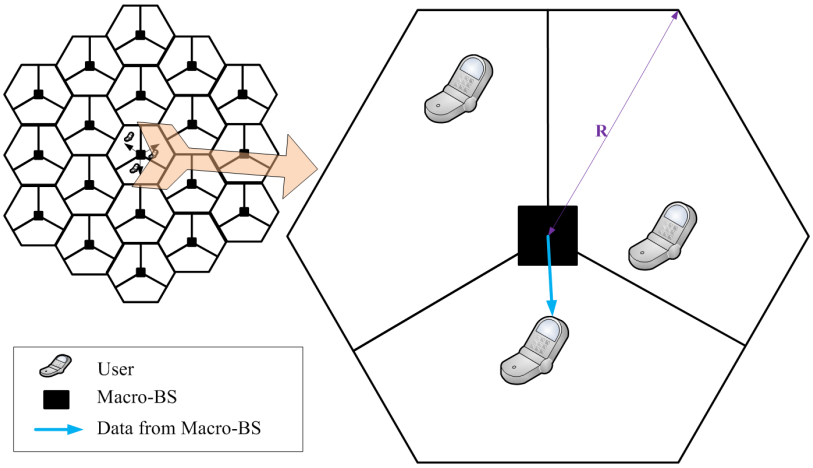

Figure 3.3: Cell architecture of MIMO systems.

(e.g. optical fiber). Hence, the desired information (e.g. CSI, transmit data) can be exchanged rapidly between the macro-BS and RRH nodes.

Two different RRH node types are considered (1) the RRH nodes share the same cell ID with the corresponding macro-BS, and (2) each RRH node has the individual cell IDs different from the corresponding macro-BS. In the former case, the macro-BS and the RRH nodes share the same single cell ID and cooperate with each other. We can regard RRH nodes as the distributed antennas within the corresponding macro-BS. In the latter case, the macro-BS and the RRH nodes with the different cell IDs are cooperated. Since each RRH node has a unique cell ID, we can regard these RRH nodes as individual low-power BSs. Each RRH node can serve their own users just as macro-BS do. There are multiple cell IDs in a cooperative set.

3.3.1 Cooperation with Single Cell ID

Based on [27], $N_H = 4$ RRH nodes fixed in every sector are regarded as the baseline and is shown in Fig. 3.4. Note that the distances between neighboring RRH nodes

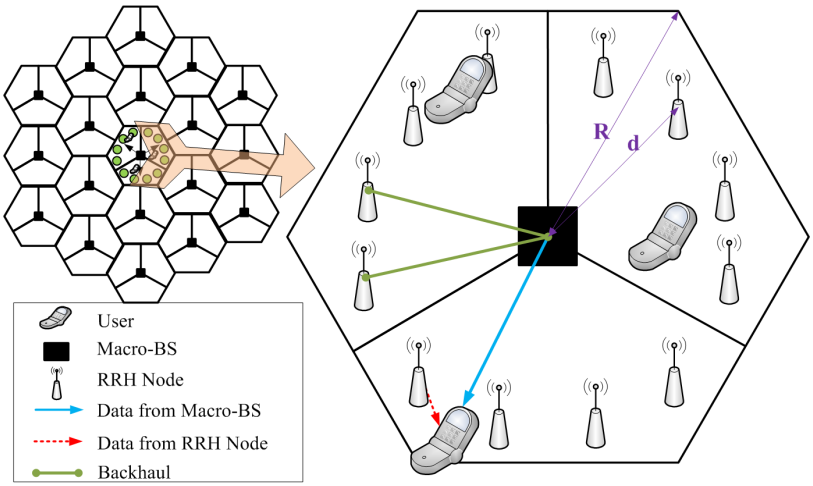

Figure 3.4: Cell architecture of the HBSC-S systesm.

are equal in our assumptions.

Since the RRH nodes share the same cell ID with the corresponding macro-BS in the HBSC-S systems, the reference signals are placed at the same resource elements (REs) and sent by the macro-BS and each RRH nodes simultaneously [28]. Let $\mathbf{H}_{s_r,b,u}^{RRH} \in \mathcal{C}^{N_r \times N_t}$ denote the channel matrix from the r^{th} RRH node in the s^{th} sector to the u^{th} user in the b^{th} sector. The u^{th} user in the b^{th} sector can only detect the effective channel $\mathbf{H}_{b,b,u}^{eff} \in \mathcal{C}^{N_r \times N_t}$, where

$$\mathbf{H}_{b,b,u}^{eff} = \mathbf{H}_{b,b,u} + \sum_{r} \mathbf{H}_{b_r,b,u}^{RRH} \ . \tag{3.9}$$

Hence, the receive signal of the u^{th} user in the b^{th} sector can be modeled as

$$\mathbf{Y}_{b,u} = \underbrace{\mathbf{H}_{b,b,u}^{eff}\mathbf{W}_{b,u}\mathbf{X}_{b,u}}_{\text{desired signal}} + \underbrace{\sum_{m \neq b} \mathbf{H}_{m,b,u}^{eff}\mathbf{W}_{m,n}\mathbf{X}_{m,n}}_{\text{inter-cell interference}} + \mathbf{n}_{b,u} \ , \tag{3.10}$$

where $\mathbf{X}_{b,u}$ denotes the desired signal of the u^{th} user in the b^{th} sector, $\mathbf{W}_{b,u}$ denotes the corresponding weighting matrix of the u^{th} user in the b^{th} sector, and $\mathbf{n}_{b,u} \in \mathcal{C}^{N_r \times 1}$ is the additive white noise with $\sigma_n^2 = -174$ dBm/Hz power density.

3.3.2 Cooperation with Multiple Cell IDs

We also fix $N_H = 4$ RRH nodes in each sector as the baseline. In the HBSC-M system, each RRH node can be regarded as an individual low-power BS within the macro-cell coverage. Hence, the RRH nodes can serve its own users just as a macro-BS do. For simplicity, we call users served by the the RRH node as RRH-users, and those by macro-BS as macro-users, respectively.

However, the macro-users and RRH-users suffer extra intra-cell interference from the RRH nodes and macro-BS, respectively. Assume that the t^{th} user is served by the r^{th} RRH node and the u^{th} user is served by the b^{th} macro-BS. Denote $\mathbf{H}_{s_r,b,t}^{RRH} \in \mathcal{C}^{N_r \times N_t}$ as the channel from the r^{th} RRH nodes in the s^{th} sector to the t^{th} RRH-user in the b^{th} sector, $\mathbf{X}_{b_r,t}^{RRH}$ as the desired signal of the t^{th} RRH-user served by the r^{th} RRH node in the b^{th} sector, and $\mathbf{W}_{b_r,t}^{RRH}$ as the corresponding weighting matrix. Hence, we can model the receive signal $\mathbf{Y}_{b_r,t}^{RRH}$ for the t^{th} user as

$$\mathbf{Y}_{b_r,t}^{RRH} = \underbrace{\mathbf{H}_{b_r,b,t}^{RRH}\mathbf{W}_{b_r,t}^{RRH}\mathbf{X}_{b_r,t}^{RRH}}_{\text{desired signal}} + \underbrace{\sum_{m}\mathbf{H}_{m,b,t}\mathbf{W}_{m,n}\mathbf{X}_{m,n}}_{\text{interference from macro-BSs}} + \underbrace{\sum_{m\neq b}\mathbf{H}_{m_k,b,t}^{RRH}\mathbf{W}_{m_k,b,t}^{RRH}\mathbf{X}_{m_k,b,t}^{RRH}}_{\text{interference from RRH nodes}} + \mathbf{n}_{b_r,t}^{RRH} \quad , \tag{3.11}$$

where $\mathbf{n}_{b_r,t}^{RRH}$ is the additive white noise with $\sigma_n^2 = -174$ dBm/Hz power density. Note that the second term in right hand side of (3.11) is the inter-cell interference from the all the macro-BSs, and the third term in the right hand side of (3.11) is the inter-cell interference from the RRH nodes in the other macro-cell.

Similarly, the received signal $\mathbf{Y}_{b,u} \in \mathcal{C}^{N_r \times 1}$ of the u^{th} user served by the b^{th} sector can be modeled as

$$\mathbf{Y}_{b,u} = \underbrace{\mathbf{H}_{b,b,u}\mathbf{W}_{b,u}\mathbf{X}_{b,u}}_{\text{desired signal}} + \underbrace{\sum_{m\neq b}\mathbf{H}_{m,b,u}\mathbf{W}_{m,n}\mathbf{X}_{m,n}}_{\text{interference from macro-BSs}}$$

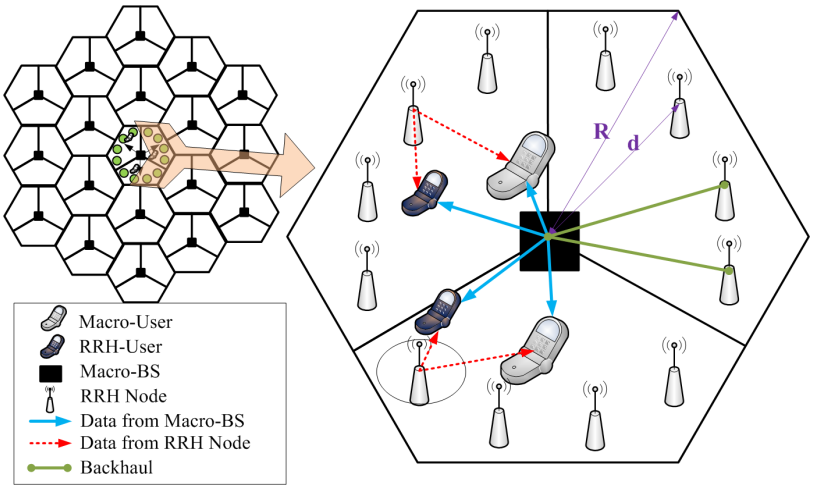

Figure 3.5: Cell architecture of the HBSC-M systesm.

$$+\underbrace{\sum_{m} \mathbf{H}^{RRH}_{m_k,b,u} \mathbf{W}^{RRH}_{m_k,b,u} \mathbf{X}^{RRH}_{m_k,b,u}}_{\text{interference from RRH nodes}} + \mathbf{n}_{b,b,u} \quad , \tag{3.12}$$

where $\mathbf{n}_{b_r,u}$ is the additive white noise with $\sigma_n^2 = -174$ dBm/Hz power density. Note that the second term in the right hand side of (3.12) is the inter-cell interference from other macro-BSs, and the third term in the right hand side of (3.12) is the inter-cell interference from all the RRH nodes in each macro-cell.

If the RRH-user and the macro-user are served by the corresponding BSs simultaneously and each user is not very close to their serving BS, strong intra-cell interference will degrade the spectral efficiency of both RRH-user and macro-user. We apply the network MIMO technique to overcome this problem. As shown in Fig. 3.5, the macro-BS and the RRH node are connected via a high speed backhaul, and work like a virtual MIMO system to jointly serve both the macro-user and RRH-user. We denote the distance between the macro-BS and each RRH node as d and the cell radius as R. Note that the distance between each neighboring RRH node is equal.

Let the t^{th} user served by the r^{th} RRH node and the u^{th} user served by the

macro-BS in the b^{th} sector are co-scheduled to apply network MIMO. Note that each RRH node shares different cell IDs with the macro-BS so that the t^{th} RRH-user can detect the channel come from the RRH node ($\mathbf{H}^{RRH}_{b_r,b,t}$), and the other channel coming from the macro-BS ($\mathbf{H}_{b,b,t}$). Similarly, the u^{th} macro-user can detect the channel coming from the macro-BS ($\mathbf{H}_{b,b,u}$), and the other channel coming from the RRH node ($\mathbf{H}^{RRH}_{b_r,b,u}$). If we regard these coordinated nodes as a virtual MIMO system, a combined channel matrix of the co-scheduled users can be respectively written as $\mathbf{H}^{com}_{b,b,t}$ and $\mathbf{H}^{com}_{b,b,u}$, where

$$\mathbf{H}^{com}_{b,b,t} = \begin{bmatrix} \mathbf{H}^{RRH}_{b_r,b,t} & \mathbf{H}_{b,b,t} \end{bmatrix} \quad , \tag{3.13}$$

and

$$\mathbf{H}^{com}_{b,b,u} = \begin{bmatrix} \mathbf{H}^{RRH}_{b_r,b,u} & \mathbf{H}_{b,b,u} \end{bmatrix} \quad . \tag{3.14}$$

Hence, we can rewrite the receive signal $\mathbf{Y}_{b,t}$ of the t^{th} RRH-user in the b^{th} sector as

$$\mathbf{Y}_{b,t} = \underbrace{\mathbf{H}^{com}_{b,b,t}\mathbf{W}_{b,t}\mathbf{X}_{b,t}}_{\text{desired signal}} + \underbrace{\mathbf{H}^{com}_{b,b,t}\mathbf{W}_{b,u}\mathbf{X}_{b,u}}_{\text{inter-user interference}}$$

$$+ \underbrace{\sum_{m\neq b}\left(\mathbf{H}^{com}_{m,b,t}\mathbf{W}_{m,n}\mathbf{X}_{m,n} + \mathbf{H}^{com}_{m,b,t}\mathbf{W}_{m,k}\mathbf{X}_{m,k}\right)}_{\text{inter-cell interference}} + \mathbf{n}_{b,t} \quad , \tag{3.15}$$

where $\mathbf{X}_{b,t}$ is the desired signal of the t^{th} RRH-user, $\mathbf{W}_{b,t}$ is the corresponding weighting matrix, and $\mathbf{n}_{b,t}$ is the additive white noise with $\sigma^2_n = -174$ dBm/Hz power density. Note that the second term in the right hand side of (3.15) is the inter-user interference, and the third term in the right hand side of (3.15) is the interference from other cooperative sets. Similarly, we can write the receive signal $\mathbf{Y}_{b,u}$ of the uth

macro-user in the b^{th} sector as

$$\mathbf{Y}_{b,u} = \underbrace{\mathbf{H}^{com}_{b,b,u}\mathbf{W}_{b,u}\mathbf{X}_{b,u}}_{desired\ signal} + \underbrace{\mathbf{H}^{com}_{b,b,u}\mathbf{W}_{b,t}\mathbf{X}_{b,t}}_{\text{inter}-\text{user interference}}$$

$$+ \underbrace{\sum_{m\neq b}\left(\mathbf{H}^{com}_{m,b,u}\mathbf{W}_{m,n}\mathbf{X}_{m,n} + \mathbf{H}^{com}_{m,b,u}\mathbf{W}_{m,k}\mathbf{X}_{m,k}\right)}_{\text{inter}-\text{cell interference}} + \mathbf{n}_{b,u} \quad , \tag{3.16}$$

where $\mathbf{X}_{b,u}$ is the desired signal of the u^{th} macro-user, $\mathbf{W}_{b,u}$ is the corresponding weighting matrix, and $\mathbf{n}_{b,u}$ is the additive white noise with $\sigma_n^2 = -174$ dBm/Hz power density. Note that the second term in the right hand side of (3.16) is the inter-user interference, and the third term in the right hand side of (3.16) is the interference from other cooperative sets.

3.4 Power Consumption Model

In order to further discuss the energy-efficiency issues, a suitable model for power consumptions is important. We have discussed three different nodes in the previous sections, i.e. the macro-BS, the RRH node with the same cell ID as the macro-BS, and the RRH node with different cell IDs from the macro-BS. Thus, we consider three different power models for each node.

Generally, the total power consumed at each BS can be divided into several parts [29]. Denoting P_{total} as the total power consumed at the BS, we can model the total consumed power per BS as

$$P_{total} = N_t \times \left(\frac{P_{Tx}}{\mu_{pa}} + P_{sp}\right) \times \beta_c \times \beta_p + P_{bh} \quad , \tag{3.17}$$

where N_t denotes the number of transmit antennas, μ_{pa} denotes the power amplifier efficiency, P_{sp} denotes the power used for signal processing, β_c denotes the additional consumed power for cooling, β_p denotes the additional consumed power for power

supply loss, and P_{bh} denotes the consumed power for exchanging the data via the backhaul. Note that $\mu_{pa} \leq 1$, $\beta_c \geq 1$, and $\beta_p \geq 1$.

We set the values of each parameter based on [16, 29, 30]. Power amplifiers in the macro-BS usually have better efficiency than those in the RRH nodes due to the worse hardware components in the small BSs. A various power amplifier efficiency 38% and 20% are set for the macro-BSs and RRH nodes respectively. P_{sp} is consumed by the signal processing and $P_{sp} = 58$ (Watts) is assumed. $\beta_c = 1.29$ and $\beta_p = 1.11$ model the additional power consumed for cooling and power supply loss, respectively. Note that the cooling power is not counted in RRH nodes because small BSs are not equipped with the cooling facilities. Furthermore, P_{bh} is modeled as

$$\mathrm{P_{bh}} = \frac{C_{bh}}{100 Mbits/s} \times 50 \ (Watts) \ . \tag{3.18}$$

where C_{bh} is the data rate, which is transmitted via the backhaul. It means that if we transmit the data with the rate $100 Mbits/s$, the consumed power is 50 (Watts).

After we have the total consumed power per BS, we formulate the energy efficiency metric. The bits per Joule ($bits/Joule$) metric is first introduced in [31], and widely used to estimate if the system is energy efficient [16, 29, 30, 32]. Let C_{total} denote the total throughput ($bits/s$) in the system so that the bits per Joule metric E_{total} can be written as

$$E_{total}(bits/Joule) = \frac{\mathrm{C_{total}}(bits/s)}{P_{total}(Joule/s)} \ . \tag{3.19}$$

Based on the energy efficiency metric E_{total}, we can estimate how many bits can be transmitted when consuming one Joule energy in different systems. Therefore, we evaluate the energy efficiency metrics of various systems, and show whether they are energy efficient or not.

CHAPTER 4

MIMO Physical Layer Simulation Platform

In this chapter, we discuss the procedures for evaluating the SU/MU-MIMO system level performance in the 3^{rd} Generation Partnership Project (3GPP) Long-Term Evolution Advanced (LTE-A) environment. To guarantee that the simulation results from various 3GPP partners are comparable, certain assumptions and constraints were agreed in the 3GPP Technical Specification Group (TSG) Radio Access Network (RAN) 1 meeting. Many equipment vendors have presented the consistent system level performance calibration results. However, they only provided the simulation results without including the detailed simulation procedures. Hence, we built a LTE-A SU/MU-MIMO system level simulation platform and provide the flow chart for the simulation procedures in the physical layer. Finally, we compare the cell-average spectral efficiency as well as the cell-edge performance with other existing evaluation results.

The simulation procedures are described as follows. In the beginning, we drop users uniformly into the entire macro-cell and calculate the radio effects, including the path-loss, shadowing, and antenna pattern. We then generate an urban macro spatial channel model (SCM) for each user. The serving sector for each user is selected based on the maximal reference signal received power (RSRP). That is, each user is given the serving sector that yields the maximal RSRP. In MIMO systems, each user selects

a precoding matrix indicator (PMI) and a rank indicator (RI) [33], and then feedback them to the BS. PMI is used to determine the precoding matrix, while RI is used to determine the transmission rank. At the receiver, the maximum ratio combining (MRC) and the minimum mean square error (MMSE) algorithms are adopted to demodulate the received signal. We calculate the received signal power and the inter-cell interference in the next step, after which we can derive the SINR for each subcarrier. The best modulation and coding schemes are changed adaptively based on the current channel quality indicator (CQI). Finally, we calculate the spectrum efficiency while taking into account retransmission and the downlink overhead. Figure 4.1 shows a flow chart of the simulation procedures.

4.1 Codebook-based Precoder

To fit the LTE-A MIMO system, we apply the codebook-based precoder in our simulation. In the ideal closed-loop MIMO system, each BS calculates the precoding matrix based on the current CSI by assuming that the full CSI is available at the BS. However, it is impractical for each user to feedback the full CSI because the feedback channel bandwidth is limited. In LTE-A MIMO systems, each user calculates the precoding matrix and feeds the PMI back as an index of the codebook. The codebook is designed offline, and the same codebook set exists at both the transmitter and the receiver. If users only feed the index back rather than the full precoding matirx, the feedback overhead can be sharply reduced.

The codebooks for two antenna ports and four antenna ports are defined in [34]. The codebook for two transmit antenna ports is given in Table 4.1. Because both rank-1 and rank-2 transmission schemes can be adopted for two transmit antenna ports, two kinds of codebook sets are needed. For rank-1 transmission, four codewords, i.e., $\mathbf{C}_0$,$\mathbf{C}_1$,...,$\mathbf{C}_3$, can be selected from the rank-1 codebook set. Similarly, for

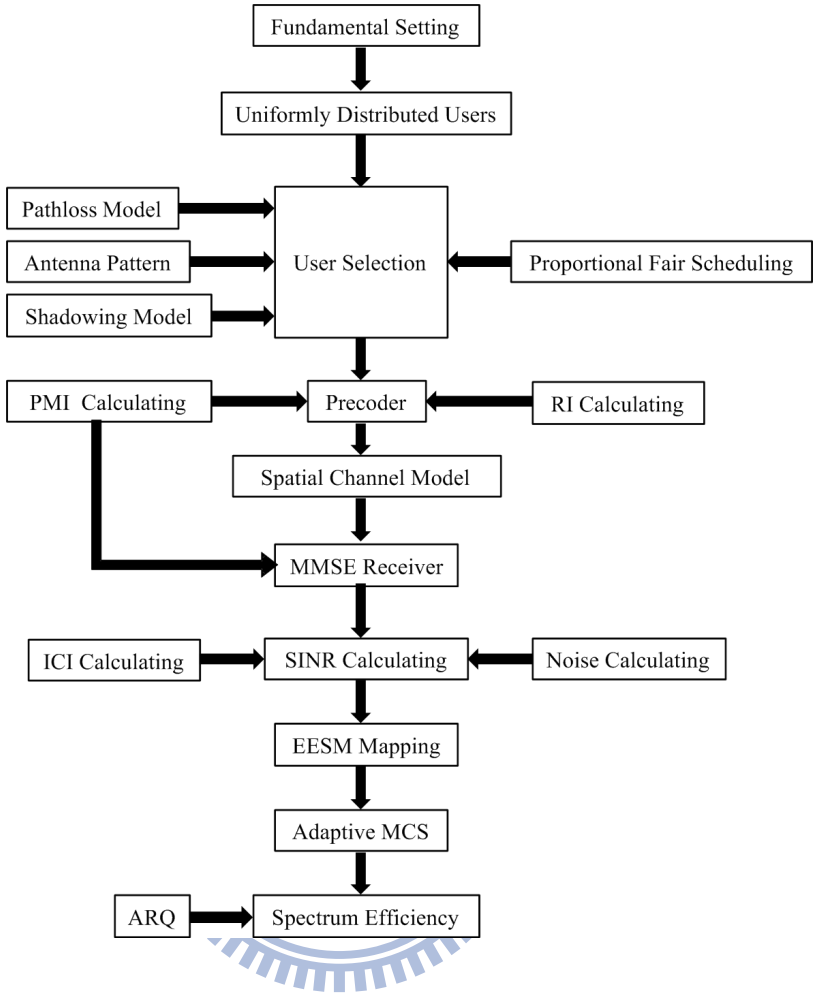

Figure 4.1: Flow chart for the physical layer simulator.

rank-2 transmission, two codewords, i.e. $\mathbf{C}_0$ and $\mathbf{C}_1$, can be selected from the rank-2 codebook set.

The codebook for four transmit antenna ports is given in Table 4.2. Sixteen codewords, i.e. $\mathbf{C}_0, \mathbf{C}_1, ..., \mathbf{C}_{15}$, can be selected from the rank-1 or the rank-2 codebook set. Note that the householder matrix $\mathbf{W}_c$ is generated by $\mathbf{u}_c$, i.e., $\mathbf{W}_c = \mathbf{I}_4 - 2\mathbf{u}_c\mathbf{u}_c^H / \mathbf{u}_c^H\mathbf{u}_c$. Note that $\mathbf{W}_c^a$ denotes the a^{th} column vector of $\mathbf{W}_c$, and $\mathbf{W}_c^{a,b}$ denotes the a^{th} and b^{th} column vectors of $\mathbf{W}_c$. Further, the Frobenius norm of each codeword

Table 4.1: **Release 9 Two Antenna Ports Codebook**

Index	**Rnak-1**	**Rnak-2**
$\mathbf{C}_0$	$\frac{1}{\sqrt{2}}\begin{bmatrix} 1 \\ 1 \end{bmatrix}$	$\frac{1}{2}\begin{bmatrix} 1 & 1 \\ 1 & -1 \end{bmatrix}$
$\mathbf{C}_1$	$\frac{1}{\sqrt{2}}\begin{bmatrix} 1 \\ -1 \end{bmatrix}$	$\frac{1}{2}\begin{bmatrix} 1 & 1 \\ j & -j \end{bmatrix}$
$\mathbf{C}_2$	$\frac{1}{\sqrt{2}}\begin{bmatrix} 1 \\ j \end{bmatrix}$	
$\mathbf{C}_3$	$\frac{1}{\sqrt{2}}\begin{bmatrix} 1 \\ -j \end{bmatrix}$	

in the codebook sets is normalized to unity because we have to preserve the same transmit power.

The precoder is calculated based on the estimated CSI at the user side. We assume that each user can perfectly estimate the CSI based on the reference signal. Hence, $\mathbf{H}_{b,b,u}$ is known at the u^{th} user in the b^{th} sector. Based on [35,36], we calculate the full precoding matrix by using the dominant eigen modes. In the case of $N_t \geq N_r$, we first decompose the channel $\mathbf{H}_{b,b,u}$ of the u^{th} user in the b^{th} sector by the using singular value decomposition (SVD) method as follows

$$\mathbf{H}_{b,b,u} = \mathbf{U}_{b,b,u}\mathbf{S}_{b,b,u}\mathbf{V}_{b,b,u}^{H} \ , \tag{4.1}$$

where

$$\mathbf{U}_{b,b,u} = \begin{bmatrix} \mathbf{u}_{b,b,u}^{1} & \cdots & \mathbf{u}_{b,b,u}^{N_r} \end{bmatrix} \in \mathcal{C}^{N_r \times N_r} \ , \tag{4.2}$$

Table 4.2: **Release 9 Four Antenna Ports Codebook**

Index	$\mathbf{u}_c$	**Rank-1**	**Rank-2**
$\mathbf{C}_0$	$\mathbf{u}_0 = \begin{bmatrix} 1 & -1 & -1 & -1 \end{bmatrix}^{\mathrm{T}}$	$\mathbf{W}_0^1$	$\mathbf{W}_0^{1,4}/\sqrt{2}$
$\mathbf{C}_1$	$\mathbf{u}_1 = \begin{bmatrix} 1 & -j & 1 & j \end{bmatrix}^{\mathrm{T}}$	$\mathbf{W}_1^1$	$\mathbf{W}_1^{1,4}/\sqrt{2}$
$\mathbf{C}_2$	$\mathbf{u}_2 = \begin{bmatrix} 1 & 1 & -1 & 1 \end{bmatrix}^{\mathrm{T}}$	$\mathbf{W}_2^1$	$\mathbf{W}_2^{1,4}/\sqrt{2}$
$\mathbf{C}_3$	$\mathbf{u}_3 = \begin{bmatrix} 1 & j & 1 & -j \end{bmatrix}^{\mathrm{T}}$	$\mathbf{W}_3^1$	$\mathbf{W}_3^{1,2}/\sqrt{2}$
$\mathbf{C}_4$	$\mathbf{u}_4 = \begin{bmatrix} 1 & (-1-j)/\sqrt{2} & -j & (1-j)/\sqrt{2} \end{bmatrix}^{\mathrm{T}}$	$\mathbf{W}_4^1$	$\mathbf{W}_4^{1,4}/\sqrt{2}$
$\mathbf{C}_5$	$\mathbf{u}_5 = \begin{bmatrix} 1 & (1-j)/\sqrt{2} & j & (1-j)/\sqrt{2} \end{bmatrix}^{\mathrm{T}}$	$\mathbf{W}_5^1$	$\mathbf{W}_5^{1,4}/\sqrt{2}$
$\mathbf{C}_6$	$\mathbf{u}_6 = \begin{bmatrix} 1 & (1+j)/\sqrt{2} & -j & (-1+j)/\sqrt{2} \end{bmatrix}^{\mathrm{T}}$	$\mathbf{W}_6^1$	$\mathbf{W}_6^{1,3}/\sqrt{2}$
$\mathbf{C}_7$	$\mathbf{u}_7 = \begin{bmatrix} 1 & (-1+j)/\sqrt{2} & j & (1+j)/\sqrt{2} \end{bmatrix}^{\mathrm{T}}$	$\mathbf{W}_7^1$	$\mathbf{W}_7^{1,3}/\sqrt{2}$
$\mathbf{C}_8$	$\mathbf{u}_8 = \begin{bmatrix} 1 & -1 & 1 & 1 \end{bmatrix}^{\mathrm{T}}$	$\mathbf{W}_8^1$	$\mathbf{W}_8^{1,2}/\sqrt{2}$
$\mathbf{C}_9$	$\mathbf{u}_9 = \begin{bmatrix} 1 & -j & -1 & -j \end{bmatrix}^{\mathrm{T}}$	$\mathbf{W}_9^1$	$\mathbf{W}_9^{1,4}/\sqrt{2}$
$\mathbf{C}_{10}$	$\mathbf{u}_{10} = \begin{bmatrix} 1 & 1 & 1 & -1 \end{bmatrix}^{\mathrm{T}}$	$\mathbf{W}_{10}^1$	$\mathbf{W}_{10}^{1,3}/\sqrt{2}$
$\mathbf{C}_{11}$	$\mathbf{u}_{11} = \begin{bmatrix} 1 & j & -1 & j \end{bmatrix}^{\mathrm{T}}$	$\mathbf{W}_{11}^1$	$\mathbf{W}_{11}^{1,3}/\sqrt{2}$
$\mathbf{C}_{12}$	$\mathbf{u}_{12} = \begin{bmatrix} 1 & -1 & -1 & 1 \end{bmatrix}^{\mathrm{T}}$	$\mathbf{W}_{12}^1$	$\mathbf{W}_{12}^{1,2}/\sqrt{2}$
$\mathbf{C}_{13}$	$\mathbf{u}_{13} = \begin{bmatrix} 1 & -1 & 1 & 1- \end{bmatrix}^{\mathrm{T}}$	$\mathbf{W}_{13}^1$	$\mathbf{W}_{13}^{1,3}/\sqrt{2}$
$\mathbf{C}_{14}$	$\mathbf{u}_{14} = \begin{bmatrix} 1 & 1 & -1 & -1 \end{bmatrix}^{\mathrm{T}}$	$\mathbf{W}_{14}^1$	$\mathbf{W}_{14}^{1,3}/\sqrt{2}$
$\mathbf{C}_{15}$	$\mathbf{u}_{15} = \begin{bmatrix} 1 & 1 & 1 & 1 \end{bmatrix}^{\mathrm{T}}$	$\mathbf{W}_{15}^1$	$\mathbf{W}_{15}^{1,2}/\sqrt{2}$

$$\mathbf{S}_{b,b,u} = \begin{bmatrix} \sigma^1_{b,b,u} & 0 & 0 & 0 & 0 & \cdots & 0 \\ 0 & \ddots & 0 & 0 & 0 & \cdots & 0 \\ \vdots & \ddots & \ddots & 0 & \vdots & \ddots & \vdots \\ 0 & \cdots & 0 & \sigma^{N_r}_{b,b,u} & 0 & \cdots & 0 \end{bmatrix} \in \mathcal{C}^{N_r \times N_t} \ , \tag{4.3}$$

and

$$\mathbf{V}^H_{b,b,u} = \begin{bmatrix} \mathbf{v}^1_{b,b,u} & \cdots & \mathbf{v}^{N_t}_{b,b,u} \end{bmatrix}^H \in \mathcal{C}^{N_t \times N_t} \ . \tag{4.4}$$

Note that $\sigma^1_{b,b,u} \geq \sigma^2_{b,b,u} \geq ... \geq \sigma^{N_r}_{b,b,u}$. If N_s data streams are transmitted to the u^{th} user simultaneously, the N_s leftmost column vectors of $\mathbf{V}_{b,b,u}$ are selected as the full precoding matirx, i.e., $\widetilde{\mathbf{W}}_{b,u}$. Thus, we can transmit the signal on the channel with a better channel quality. For example, in the SU-MIMO rank-1 system with $N_t = 2$ and $N_r = 2$, we select $\mathbf{v}^1_{b,b,u}$ as the full precoding vector $\widetilde{\mathbf{W}}_{b,b,u}$, where $\widetilde{\mathbf{W}}_{b,u}$ is the percoding vector of the u^{th} user in the b^{th} sector. Similarly, in the SU-MIMO rank-2 system with $N_t = 2$ and $N_r = 2$, we select both $\mathbf{v}^1_{b,b,u}$ and $\mathbf{v}^2_{b,b,u}$ as the full precoding matrix $\widetilde{\mathbf{W}}_{b,u}$, where $\widetilde{\mathbf{W}}_{b,b,u}$ is the percoding matrix of the u^{th} user in the b^{th} sector.

Once we have the full precoding matrix $\widetilde{\mathbf{W}}_{b,u}$, we search for the most suitable codeword to represent it since it is impractical for the user feedbacking the full precoding matrix with infinite bits. Codewords are selected based on the minimum angle between each codeword and the full precoding matrix [37, 38]

$$a = \arg\max_i trace\left(\left|\mathbf{C}_i^H \widetilde{\mathbf{W}}_{b,u}\right|\right) \ , \tag{4.5}$$

where $\mathbf{C}_i$ is the codeword defined in Tables 4.1 and 4.2, and a is the selected codeword index. Each user only feeds the index a of the corresponding codeword back. Hence, the number of feedback bits can be sharply reduced.

4.2 Receiver Structure

At the user, the MRC and MMSE receiver structures are adopted [22, 39]. The MRC receiver is used to maximize the desired receive signal power in the rank-1 SU-MIMO system, whereas the MMSE receiver is used to suppress the inter-stream and inter-user interference in the multi-rank MIMO system, where the former is caused by the multi-stream interference in SU-MIMO systems and the latter is caused by the multi-user interference in MU-MIMO systems.

In the rank-1 SU-MIMO system, the MRC receiver is adopted. Let the u^{th} user be the serving user with only one data symbol $\mathbf{X}_{b,u} = x^1_{b,u}$ transmitted. Assuming that the precoding vector $\mathbf{W}_{b,u} = \mathbf{w}^1_{b,u}$ is selected from the codebook set, we can rewrite the receive signal based on (3.8) as follows:

$$\mathbf{Y}_{b,u} = \mathbf{H}_{b,b,u}\mathbf{w}^1_{b,u}x^1_{b,u} + \sum_{m\neq b}\mathbf{H}_{m,b,u}\mathbf{W}_{m,n}\mathbf{X}_{m,n} + \mathbf{n}_{b,u} \quad . \tag{4.6}$$

The MRC receiver algorithm $\mathbf{M}^1_{b,u} \in \mathcal{C}^{1\times N_r}$ for the u^{th} user can be derived as

$$\mathbf{M}^1_{b,u} = \left[\mathbf{H}_{b,b,u}\mathbf{w}^1_{b,u}\right]^H \quad , \tag{4.7}$$

where $\mathbf{M}^1_{b,u}$ is used to demodulate the data symbol $x^1_{b,u}$ by multiplying the receive signal $\mathbf{Y}_{b,u}$ by $\mathbf{M}^1_{b,u}$.

In the rank-2 SU-MIMO system, two data symbols $\mathbf{X}_{b,u} = \begin{bmatrix} x^1_{b,u} & x^2_{b,u} \end{bmatrix}$ can be transmitted simultaneously to the single user. Let $\mathbf{W}_{b,u} = \begin{bmatrix} \mathbf{w}^1_{b,u} & \mathbf{w}^2_{b,u} \end{bmatrix}$ be the selected precoding matrix from the codebook set, and each data symbol, i.e. $x^1_{b,u}$ and $x^2_{b,u}$, is multiplied by the corresponding precoding vector $\mathbf{w}^1_{b,u}$ and $\mathbf{w}^2_{b,u}$ respectively. We can rewrite the receive signal based on (3.8) as

$$\mathbf{Y}_{b,u} = \mathbf{H}_{b,b,u}\begin{bmatrix} \mathbf{w}^1_{b,u} & \mathbf{w}^2_{b,u} \end{bmatrix}\begin{bmatrix} x^1_{b,u} & x^1_{b,u} \end{bmatrix}^T + \sum_{m\neq b}\mathbf{H}_{m,b,u}\mathbf{W}_{m,n}\mathbf{X}_{m,n} + \mathbf{n}_{b,u} \quad . \tag{4.8}$$

Then we can derive the MMSE receive algorithm, $\mathbf{M}^1_{b,u} \in \mathcal{C}^{1\times N_r}$ and $\mathbf{M}^2_{b,u} \in \mathcal{C}^{1\times N_r}$, for the u^{th} user in the b^{th} sector as

$$\mathbf{M}^1_{b,u} = \left[\left(\sigma_n^2\mathbf{I} + \mathbf{H}_{b,b,u}\mathbf{w}^2_{b,u}\left(\mathbf{H}_{b,b,u}\mathbf{w}^2_{b,u}\right)^H\right)^{-1}\mathbf{H}_{b,b,u}\mathbf{w}^1_{b,u}\right]^H \tag{4.9}$$

and

$$\mathbf{M}^2_{b,u} = \left[\left(\sigma_n^2\mathbf{I} + \mathbf{H}_{b,b,u}\mathbf{w}^1_{b,u}\left(\mathbf{H}_{b,b,u}\mathbf{w}^1_{b,u}\right)^H\right)^{-1}\mathbf{H}_{b,b,u}\mathbf{w}^2_{b,u}\right]^H \quad , \tag{4.10}$$

where $\mathbf{M}^1_{b,b,u}$ and $\mathbf{M}^2_{b,b,u}$ are used to demodulate the data symbol $x^1_{b,u}$ and $x^2_{b,u}$ by multiplying the received signal $\mathbf{Y}_{b,u}$ by $\mathbf{M}^1_{b,b,u}$ and $\mathbf{M}^2_{b,b,u}$, respectively.

In the rank-1 MU-MIMO system with $N_t = 2$ and $N_r = 2$, the BS can serve two co-scheduled users simultaneously with one data stream per user. The interference now consists of the inter-user interference. That is, the co-scheduled users interferes with each other. Let the t^{th} and u^{th} users be co-scheduled in the b^{th} sector. Assume that $\mathbf{W}_{b,t} = \mathbf{w}^1_{b,t}$ is the selected precoding vector for the t^{th} user, and $\mathbf{W}_{b,u} = \mathbf{w}^1_{b,u}$ is the selected precoding vector for the u^{th} user. Then, each data symbol, $\mathbf{X}_{b,t} = x^1_{b,t}$ for the t^{th} user and $\mathbf{X}_{b,u} = x^1_{b,u}$ for the u^{th} user, is multiplied by the corresponding precoding vector. We can rewrite the receive signal (3.8) for the t^{th} and u^{th} users as follows:

$$\mathbf{Y}_{b,t} = \mathbf{H}_{b,b,t}\mathbf{w}^1_{b,t}x^1_{b,t} + \mathbf{H}_{b,b,t}\mathbf{w}^1_{b,u}x^1_{b,u} + \sum_{m\neq b}\mathbf{H}_{m,b,t}\mathbf{W}_{m,n}\mathbf{X}_{m,n} + \mathbf{n}_{b,t} \tag{4.11}$$

and

$$\mathbf{Y}_{b,u} = \mathbf{H}_{b,b,u}\mathbf{w}^1_{b,u}x^1_{b,u} + \mathbf{H}_{b,b,u}\mathbf{w}^1_{b,t}x^1_{b,t} + \sum_{m\neq b}\mathbf{H}_{m,b,u}\mathbf{W}_{m,n}\mathbf{X}_{m,n} + \mathbf{n}_{b,u} \quad . \tag{4.12}$$

The MMSE receive algorithm, $\mathbf{M}^1_{b,b,t} \in \mathcal{C}^{1\times N_r}$ and $\mathbf{M}^2_{b,b,u} \in \mathcal{C}^{1\times N_r}$, for the t^{th} and u^{th} users can be derived as follows

$$\mathbf{M}^1_{b,t} = \left[\left(\sigma_n^2\mathbf{I} + \mathbf{H}_{b,b,t}\mathbf{w}^1_{b,u}\left(\mathbf{H}_{b,b,t}\mathbf{w}^1_{b,u}\right)^H\right)^{-1}\mathbf{H}_{b,b,t}\mathbf{w}^1_{b,t}\right]^H \tag{4.13}$$

and

$$\mathbf{M}_{b,u}^{1} = \left[\left(\sigma_n^2 \mathbf{I} + \mathbf{H}_{b,b,u} \mathbf{w}_{b,t}^{1} \left(\mathbf{H}_{b,b,u} \mathbf{w}_{b,t}^{1} \right)^H \right)^{-1} \mathbf{H}_{b,b,u} \mathbf{w}_{b,u}^{1} \right]^H , \tag{4.14}$$

where $\mathbf{M}_{b,b,t}^{1}$ and $\mathbf{M}_{b,b,u}^{1}$ are used to demodulate the data symbol $x_{b,t}^{1}$ and $x_{b,u}^{1}$ by multiplying the receive signal $\mathbf{Y}_{b,t}$ and $\mathbf{Y}_{b,u}$ by $\mathbf{M}_{b,b,t}^{1}$ and $\mathbf{M}_{b,b,u}^{1}$, respectively.

4.3 Rank Adaptation and SU/MU-MIMO Switching

The transmission rank adaptation technique is widely used in 3GPP LTE-A MIMO systems [40–44]. Generally, each user need to determine the transmission rank and feedback it to the BS. Spatial multiplexing for higher rank can significantly improve spectrum efficiency in the high SINR regime. However, when channel quality is low, spatial multiplexing may degrade the performance. Hence, lower rank transmission is applied to enhance the cell-edge spectral efficiency [45]. We adopt ideal rank adaptation in our simulations. That is, we find out which transmission rank can yield the highest spectral efficiency and then adopt that transmission rank.

MU-MIMO is an advanced technology where a BS serves multiple users (co-scheduled users) in the same resource block (RB) by exploiting degrees of freedom in the spatial domain. Hence, the spectral efficiency increases. However, the co-scheduled users are not always compatible to be co-scheduled because of the CSI. Namely, those users whose CSI is sufficiently orthogonal to each other are suitable for co-scheduling. Therefore, to further enhance the spectral efficiency in the MU-MIMO systems, a switching technique between the SU-MIMO mode and the MU-MIMO mode is prerequisite [42, 46, 47]. In [42], it was shown that we could have obtained a gain of approximately 21% as compared to SU-MIMO systems by applying the SU/MU-MIMO switching techniques. Thus, we apply the ideal SU/MU switching

techniques in our simulation. That is, we determine which transmission mode can yield the highest spectral efficiency and then adopt that transmission mode. Note that in the $N_t = 2$ and $N_r = 2$ MU-MIMO system, we apply both rank adaptation and SU/MU-MIMO switching techniques simultaneously, where the rank per user is up to two for the SU-MIMO mode, and the rank per user is up to one for the MU-MIMO mode.

4.4 Proportional Fair Scheduling

Proportional fair (PF) scheduling is applied in the SU-MIMO and MU-MIMO systems. If we want to find the best cell-average spectral efficiency, the users in the center of the cell are always served. Thus, cell-edge users may obtain no resources for a long time which is an unfair situation for them. Proportional fair scheduling is a joint design that can ensure the fairness and a good transmission rate. The user is served if the current transmission rate is high or the past average transmission rate is low. By considering proportional fair scheduling, we can avoid the situation where the cell-edge user is never served.

For SU-MIMO systems, we consider both the current transmission rate and the past average transmission rate as follows

$$a_s = \arg\max_u \frac{R_{u,r}}{T_{u,\hat{r}}}, u = 1, 2, ..., N_u \ , \tag{4.15}$$

where $R_{u,r}$ denotes the current transmission rate of the u^{th} user in the r^{th} RB, $T_{u,\hat{r}}$ denotes the past average transmission rate of the u^{th} user before the r^{th} RB, and the index a_s denotes that the a_s^{th} user is selected to serve in the r^{th} RB.

For MU-MIMO systems, we assume that there are N_g co-scheduled groups with each consisting of N_{gu} users. We consider both the current transmission rate

and the past average transmission rate to select the users

$$a_m = \arg\max_{m} \sum_{u=1}^{N_{gu}} \frac{R_{u,r}^{m}}{T_{u,\hat{r}}^{m}}, m = 1, 2, ...N_g \ , \tag{4.16}$$

where $R_{u,r}^{m}$ denotes the current transmission rate of the u^{th} user within the m^{th} co-scheduled group in the r^{th} RB, $T_{u,\hat{r}}^{m}$ denotes the past average transmission rate of the u^{th} user within the m^{th} co-scheduled group before the r^{th} RB, and the index a_m denotes that all the users within a_m^{th} group are served jointly in the r^{th} RB.

CHAPTER 5

Hierarchical Base Station Cooperation Simulation Platform

In this chapter, we discuss the simulation procedures of hierarchical base station cooperation systems (HBSC). Recall that two systems are considered (1) the RRH nodes share the same cell ID with the corresponding macro-BS (HBSC-S) and (2) the RRH nodes have multiple cell IDs different from the corresponding macro-BS (HBSC-M).

5.1 RRH Nodes Selection

5.1.1 Cooperation with Single Cell ID

In HBSC-S systems, each user selects the suitable RRH node be the serving nodes. We apply an RSRP-based RRH nodes selection algorithm. Since the users are uniformly distributed in the cell, each user may be closer to certain RRH node and farther away from the other RRH nodes. The received power contributed by the RRH nodes that are farther away from the serving user is quite low. Hence, we switch off the useless RRH nodes and only switch on a certain number of RRH nodes to serve the users. Let $N_{HS} \leq N_H$ denotes the number of RRH nodes selected to serve the user. For the u^{th} user in the b^{th} sector, we select the N_{HS} largest RSRPs from the RSRP set

$\mathbf{P}^{RSRP}_{b_{N_H},b,u} = \left\{P^{RSRP}_{b_1,b,u}, P^{RSRP}_{b_2,b,u}, ..., P^{RSRP}_{b_{N_H},b,u}\right\}$, where $P^{RSRP}_{b_r,b,u}$ is the RSRP of the u^{th} user from the r^{th} RRH node in the b^{th} sector. Then, the N_{HS} corresponding RRH nodes are selected to serve the user. For example, if $N_{HS} = 2$ and $P^{RSRP}_{b_1,b,u} \geq P^{RSRP}_{b_2,b,u} \geq ... \geq P^{RSRP}_{b_{N_H},b,u}$, the first and the second RRH nodes in the b^{th} sector are selected to serve the u^{th} user.

5.1.2 Cooperation with Multiple Cell IDs

In HBSC-M systems, we need to determine that each user is served by the macro-BS or RRH nodes. In our considerations, users served by the macro-BS are assigned to the macro-user set and users served by the RRH node are assigned to the RRH-user set, where the former consists of all macro-user and the latter consists of all RRH-users. We pair two users, i.e. one macro-user and one RRH-user each, as a cooperation group. The users within the cooperation group are served jointly by the macro-BS and the RRH node. In order to match the previous simulation assumptions, we still uniformly drop N_u users into each sector.

Users are assigned to each set based on the maximum RSRP. We define the RSRP set $\mathbf{P}^{RSRP}_{b,b,u} = \left\{P^{RSRP}_{b,b,u}, P^{RSRP}_{b_1,b,u}, P^{RSRP}_{b_2,b,u}, ..., P^{RSRP}_{b_{N_H},b,u}\right\}$ for the u^{th} user, where $P^{RSRP}_{b,b,u}$ is the RSRP for the u^{th} user form the b^{th} macro-BS and $P^{RSRP}_{b_r,b,u}$ is the RSRP for the u^{th} user from the r^{th} RRH node in the b^{th} sector. In the first step, we search the largest RSRP for each user. If

$$\max\left(\mathbf{P}^{RSRP}_{b,b,u}\right) = P^{RSRP}_{b,b,u},\ u = 1, 2, ..., N_u\ , \tag{5.1}$$

the u^{th} user is assigned the the macro-user set and is served by the b^{th} macro-BS. On the contrary, if

$$\max\left(\mathbf{P}^{RSRP}_{b,b,u}\right) = P^{RSRP}_{b_r,b,u},\ u = 1, 2, ..., N_u\ , \tag{5.2}$$

the u^{th} user is assigned the the RRH-user set and is served by the r^{th} RRH node in the b^{th} sector. Based on the above procedures, we can always find the users that have better channels to one BS. Moreover, based on [48,49], only one RRH node within the sector can work in the mean time for avoiding that RRH nodes interfere with each other. That is, if the r^{th} RRH node is serving users in the b^{th} sector, the remaining RRH nodes in the same sector stop transmitting data.

5.2 Transmit Signal Model

5.2.1 Cooperation with Single Cell ID

Let $\mathbf{H}_{s_r,b,u}^{RRH} \in \mathcal{C}^{N_r \times N_t}$ denote the channel matrix from the r^{th} RRH node in the s^{th} sector to the u^{th} user in the b^{th} sector. Recall that the RRH nodes share the same cell ID with the corresponding macro-BS. Thus, the reference signals are placed at the same REs and sent by the macro-BS and each RRH nodes simultaneously. Therefore, the u^{th} user can only detect the effective channel $\mathbf{H}_{b,b,u}^{eff} \in \mathcal{C}^{N_r \times N_t}$, where $\mathbf{H}_{b,b,u}^{eff} = \mathbf{H}_{b,b,u} + \sum_{r=1}^{N_{HS}} \mathbf{H}_{b_r,b,u}^{RRH}$.

The precoding matrix is calculated based on the estimated CSI at the user. We assume that each user can perfectly estimate the CSI based on the reference signal. Hence, $\mathbf{H}_{b,b,u}^{eff}$ is known at the u^{th} user in the b^{th} sector. We calculate the full precoding matrix using the dominant eigen modes. For $N_t \geq N_r$, the u^{th} user then decomposes the effective channel $\mathbf{H}_{b,b,u}^{eff}$ by using the SVD method as

$$\mathbf{H}_{b,b,u}^{eff} = \mathbf{U}_{b,b,u}\mathbf{S}_{b,b,u}\mathbf{V}_{b,b,u}^{H} \ , \tag{5.3}$$

where

$$\mathbf{U}_{b,b,u} = \left[\begin{array}{ccc} \mathbf{u}_{b,b,u}^{1} & \cdots & \mathbf{u}_{b,b,u}^{N_r} \end{array} \right] \in \mathcal{C}^{N_r \times N_r} \ , \tag{5.4}$$

$$\mathbf{S}_{b,b,u} = \begin{bmatrix} \sigma^1_{b,b,u} & 0 & 0 & 0 & 0 & \cdots & 0 \\ 0 & \ddots & 0 & 0 & 0 & \cdots & 0 \\ \vdots & \ddots & \ddots & 0 & \vdots & \ddots & \vdots \\ 0 & \cdots & 0 & \sigma^{N_r}_{b,b,u} & 0 & \cdots & 0 \end{bmatrix} \in \mathcal{C}^{N_r \times N_t} \ , \tag{5.5}$$

and

$$\mathbf{V}^H_{b,b,u} = \begin{bmatrix} \mathbf{v}^1_{b,b,u} & \cdots & \mathbf{v}^{N_t}_{b,b,u} \end{bmatrix}^H \in \mathcal{C}^{N_t \times N_t} \ . \tag{5.6}$$

Note that $\sigma^1_{b,b,u} \geq \sigma^2_{b,b,u} \geq ... \geq \sigma^{N_r}_{b,b,u}$. If N_s data streams are transmitted to the u^{th} user simultaneously, the N_s leftmost column vectors of $\mathbf{V}_{b,b,u}$ are selected as the full precoding matrix, i.e., $\widetilde{\mathbf{W}}_{b,u}$, due to the better channel quality.

5.2.2 Cooperation with Multiple Cell IDs

Since the RRH-user and the macro-user may be very close to their serving BSs, these users can obtain higher capacity if we do not cooperate the nodes as shown in Fig. 5.1. Hence, switching between the cooperation mode and non-cooperation mode is needed to improve spectral efficiency. We consider the ideal two-mode switching technique in our system. That is, we always select the best mode that yields the maximum sum rate.

For the cooperation mode, we first calculate the full precoding matrix by using the dominant eigen modes. Assume that the t^{th} user is served by the r^{th} RRH node in the b^{th} sector, the u^{th} user is served by the macro-BS in the b^{th} sector, and both the t^{th} and u^{th} users are co-scheduled to apply cooperation transmission. The t^{th} RRH-user decomposes the combined channel $\mathbf{H}^{com}_{b,b,t}$ by using the SVD method

$$\mathbf{H}^{com}_{b,b,t} = \mathbf{U}_{b,b,t}\mathbf{S}_{b,b,t}\mathbf{V}^H_{b,b,t} \ , \tag{5.7}$$

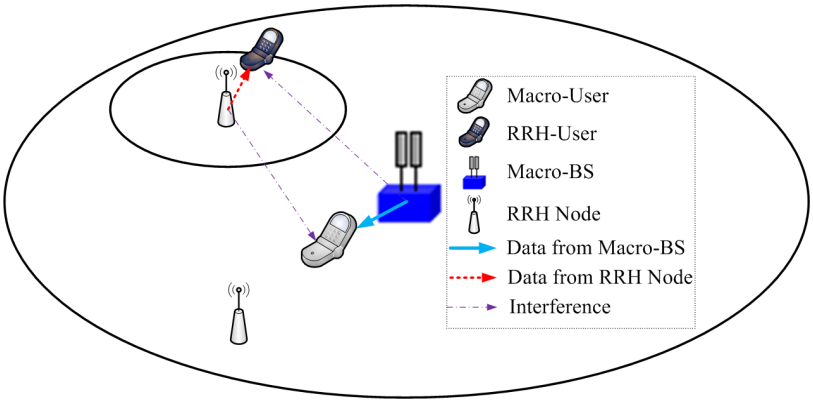

Figure 5.1: Non-cooperation transmission mode in the hierarchical system.

where

$$\mathbf{U}_{b,b,t} = \begin{bmatrix} \mathbf{u}^1_{b,b,u} & \cdots & \mathbf{u}^{N_r}_{b,b,t} \end{bmatrix}, \tag{5.8}$$

$$\mathbf{S}_{b,b,t} = \begin{bmatrix} \sigma^1_{b,b,t} & 0 & 0 & 0 & 0 & \cdots & 0 \\ 0 & \ddots & 0 & 0 & 0 & \cdots & 0 \\ \vdots & \ddots & \ddots & 0 & \vdots & \ddots & \vdots \\ 0 & \cdots & 0 & \sigma^{N_r}_{b,b,t} & 0 & \cdots & 0 \end{bmatrix}, \tag{5.9}$$

and

$$\mathbf{V}^H_{b,b,t} = \begin{bmatrix} \mathbf{v}^1_{b,b,t} & \cdots & \mathbf{v}^{2\times N_t}_{b,b,t} \end{bmatrix}^H. \tag{5.10}$$

Note that $\sigma^1_{b,b,t} \geq \sigma^2_{b,b,t} \geq ... \geq \sigma^{N_r}_{b,b,t}$. If N_s data streams are transmitted to the t^{th} RRH-user simultaneously, the N_s leftmost column vectors of $\mathbf{V}_{b,b,t}$ are selected as the full precoding matirx, i.e., $\widetilde{\mathbf{W}}_{b,t}$. Similarly, the u^{th} macro-user decomposes the combined channel $\mathbf{H}^{com}_{b,b,u}$ by using SVD method and then obtains the full precoding matrix in the same way.

For the non-cooperation mode, the RRH node and the macro-BS do not serve users jointly. We individually calculate the full precoding matrix for each RRH-user and macro-user respectively. In the $N_t \geq N_r$ case, the t^{th} RRH-user, which is served by the r^{th} RRH node, decomposes the channel $\mathbf{H}_{b_r,b,t}$ by using the SVD method as

$$\mathbf{H}_{b_r,b,t} = \mathbf{U}_{b,b,t}\mathbf{S}_{b,b,t}\mathbf{V}_{b,b,t}^{H} \ , \tag{5.11}$$

where

$$\mathbf{U}_{b,b,t} = \begin{bmatrix} \mathbf{u}_{b,b,t}^{1} & \cdots & \mathbf{u}_{b,b,t}^{N_r} \end{bmatrix} \ , \tag{5.12}$$

$$\mathbf{S}_{b,b,t} = \begin{bmatrix} \sigma_{b,b,t}^{1} & 0 & 0 & 0 & 0 & \cdots & 0 \\ 0 & \ddots & 0 & 0 & 0 & \cdots & 0 \\ \vdots & \ddots & \ddots & 0 & \vdots & \ddots & \vdots \\ 0 & \cdots & 0 & \sigma_{b,b,t}^{N_r} & 0 & \cdots & 0 \end{bmatrix} \ , \tag{5.13}$$

and

$$\mathbf{V}_{b,b,t}^{H} = \begin{bmatrix} \mathbf{v}_{b,b,t}^{1} & \cdots & \mathbf{v}_{b,b,t}^{N_t} \end{bmatrix}^{H} \ . \tag{5.14}$$

Note that $\sigma_{b,b,t}^{1} \geq \sigma_{b,b,t}^{2} \geq ... \geq \sigma_{b,b,t}^{N_r}$. If N_s data streams are transmitted to the t^{th} user simultaneously, the N_s leftmost column vectors of $\mathbf{V}_{b,b,t}$ are selected as the full precoding matrix, i.e. $\widetilde{\mathbf{W}}_{b,t}$. Similarly, the u^{th} macro-user decomposes the channel $\mathbf{H}_{b,b,u}$ by the using SVD method and obtains the full precoding matrix in the same way. Note that in the non-cooperation mode, the t^{th} RRH-user interferes with the u^{th} macro-user, and vice versa.

Once we have the full percoding matrix, we then search the suitable codebook just as in Section 4.1.

5.3 Receiver Structure

5.3.1 Cooperation with Single Cell ID

In the rank-1 HBSC-S system, the MRC receiver is adopted. Let the u^{th} user be the serving user with only one data symbol $\mathbf{X}_{b,u} = x^1_{b,u}$ transmitted. Assuming that the precoding vector $\mathbf{W}_{b,u} = \mathbf{w}^1_{b,u}$ is selected from the codebook set, we can rewrite the receive signal based on (3.10) as :

$$\mathbf{Y}_{b,u} = \mathbf{H}^{eff}_{b,b,u}\mathbf{w}^1_{b,u}x^1_{b,u} + \sum_{m\neq b}\mathbf{H}^{eff}_{m,b,u}\mathbf{W}_{m,n}\mathbf{X}_{m,n} + \mathbf{n}_{b,u} \ . \tag{5.15}$$

The MRC receive algorithm, $\mathbf{M}^1_{b,b,u} \in 1 \times \mathcal{C}^{N_r}$, for the u^{th} user can be derived as :

$$\mathbf{M}^1_{b,u} = \left[\mathbf{H}^{eff}_{b,b,u}\mathbf{w}^1_{b,u}\right]^H \ , \tag{5.16}$$

where $\mathbf{M}^1_{b,u}$ is used to detect the symbol $x^1_{b,u}$ by multiplying the received signal $\mathbf{Y}_{b,u}$ by $\mathbf{M}^1_{b,u}$.

In the rank-2 HBSC-S system, two data symbols $\mathbf{X}_{b,u} = \begin{bmatrix} x^1_{b,u} & x^2_{b,u} \end{bmatrix}$ can be transmitted simultaneously to the u^{th} user. Let $\mathbf{W}_{b,u} = \begin{bmatrix} \mathbf{w}^1_{b,u} & \mathbf{w}^2_{b,u} \end{bmatrix}$ be the selected precoding matrix from the codebook set with each data symbol, i.e. $x^1_{b,u}$ and $x^2_{b,u}$, is multiplied by the corresponding precoding vector. Thus, the receive signal in (3.10) can be rewritten as

$$\mathbf{Y}_{b,u} = \mathbf{H}^{eff}_{b,b,u}\begin{bmatrix} \mathbf{w}^1_{b,u} & \mathbf{w}^2_{b,u} \end{bmatrix}\begin{bmatrix} x^1_{b,u} & x^1_{b,u} \end{bmatrix}^T + \sum_{m\neq b}\mathbf{H}^{eff}_{m,b,u}\mathbf{W}_{m,n}\mathbf{X}_{m,n} + \mathbf{n}_{b,u} \ . \tag{5.17}$$

We can derive the MMSE receive algorithm, $\mathbf{M}^1_{b,b,u} \in 1 \times \mathcal{C}^{N_r}$ and $\mathbf{M}^2_{b,b,u} \in 1 \times \mathcal{C}^{N_r}$, for the u^{th} user as

$$\mathbf{M}^1_{b,u} = \left[\left(\sigma^2_n\mathbf{I} + \mathbf{H}^{eff}_{b,b,u}\mathbf{w}^2_{b,u}\left(\mathbf{H}^{eff}_{b,b,u}\mathbf{w}^2_{b,u}\right)^H\right)^{-1}\mathbf{H}^{eff}_{b,b,u}\mathbf{w}^1_{b,u}\right]^H \tag{5.18}$$

and

$$\mathbf{M}_{b,u}^{2} = \left[\left(\sigma_n^2 \mathbf{I} + \mathbf{H}_{b,b,u}^{eff} \mathbf{w}_{b,u}^{1} \left(\mathbf{H}_{b,b,u}^{eff} \mathbf{w}_{b,u}^{1} \right)^{H} \right)^{-1} \mathbf{H}_{b,b,u}^{eff} \mathbf{w}_{b,u}^{2} \right]^{H} , \tag{5.19}$$

where $\mathbf{M}_{b,u}^{1}$ and $\mathbf{M}_{b,u}^{2}$ are used to detect the symbols $x_{b,u}^{1}$ and $x_{b,u}^{2}$ by multiplying the receive signal $\mathbf{Y}_{b,u}$ by $\mathbf{M}_{b,u}^{1}$ and $\mathbf{M}_{b,u}^{2}$, respectively.

5.3.2 Cooperation with Multiple Cell IDs

Recall that we switch the transmission mode between network MIMO mode and non-network MIMO mode. Therefore, we adaptively change the receiver structure based on the transmission mode.

For the rank-1 HBSC-M systems, two data streams, $\mathbf{X}_{b,t} = x_{b,t}^{1}$ and $\mathbf{X}_{b,u} = x_{b,u}^{1}$, can be transmitted jointly to the t^{th} RRH-user and the u^{th} macro-user repectively. Let $\mathbf{W}_{b,t} = \mathbf{w}_{b,t}^{1} \in \mathcal{C}^{1\times 2N_t}$ and $\mathbf{W}_{b,u} = \mathbf{w}_{b,u}^{1} \in \mathcal{C}^{1\times 2N_t}$ denote corresponding precoding vectors. Each data symbol $\mathbf{X}_{b,t} = x_{b,t}^{1}$ and $\mathbf{X}_{b,u} = x_{b,u}^{1}$ is multiplied by the corresponding precoding vector. We can rewrite the receive signals based on (3.15) and (3.16) as follows

$$\mathbf{Y}_{b,t} = \mathbf{H}_{b,b,t}^{com} \mathbf{w}_{b,t}^{1} x_{b,t}^{1} + \mathbf{H}_{b,b,t}^{com} \mathbf{w}_{b,u}^{1} x_{b,u}^{1} + \sum_{m\neq b} \left(\mathbf{H}_{m,b,t}^{com} \mathbf{W}_{m,n} \mathbf{X}_{m,n} + \mathbf{H}_{m,b,t}^{com} \mathbf{W}_{m,k} \mathbf{X}_{m,k} \right) + \mathbf{n}_{b,t} , \tag{5.20}$$

and

$$\mathbf{Y}_{b,u} = \mathbf{H}_{b,b,u}^{com} \mathbf{w}_{b,u}^{1} x_{b,u}^{1} + \mathbf{H}_{b,b,u}^{com} \mathbf{w}_{b,t}^{1} x_{b,t}^{1} + \sum_{m\neq b} \left(\mathbf{H}_{m,b,u}^{com} \mathbf{W}_{m,n} \mathbf{X}_{m,n} + \mathbf{H}_{m,b,u}^{com} \mathbf{W}_{m,k} \mathbf{X}_{m,k} \right) + \mathbf{n}_{b,u} . \tag{5.21}$$

We can derive the MMSE receive algorithm, $\mathbf{M}_{b,b,t}^{1} \in 1 \times \mathcal{C}^{N_r}$ and $\mathbf{M}_{b,b,u}^{1} \in 1 \times \mathcal{C}^{N_r}$, for the t^{th} RRH-user and the u^{th} macro-user in the b^{th} sector as follows

$$\mathbf{M}_{b,t}^{1} = \left[\left(\sigma_n^2 \mathbf{I} + \mathbf{H}_{b,b,t}^{com} \mathbf{w}_{b,u}^{1} \left(\mathbf{H}_{b,b,t}^{com} \mathbf{w}_{b,u}^{1} \right)^{H} \right)^{-1} \mathbf{H}_{b,b,t}^{com} \mathbf{w}_{b,t}^{1} \right]^{H} \tag{5.22}$$

and

$$\mathbf{M}_{b,u}^{1} = \left[\left(\sigma_n^2 \mathbf{I} + \mathbf{H}_{b,b,u}^{com} \mathbf{w}_{b,t}^{1} \left(\mathbf{H}_{b,b,u}^{com} \mathbf{w}_{b,t}^{1} \right)^H \right)^{-1} \mathbf{H}_{b,b,u}^{eff} \mathbf{w}_{b,u}^{1} \right]^H , \tag{5.23}$$

where $\mathbf{M}_{b,b,t}^{1}$ and $\mathbf{M}_{b,b,u}^{1}$ are used to detect the data symbols $x_{b,t}^{1}$ and $x_{b,u}^{2}$ by multiplying the receive signals $\mathbf{Y}_{b,t}$ and $\mathbf{Y}_{b,u}$ by $\mathbf{M}_{b,b,t}^{1}$ and $\mathbf{M}_{b,b,u}^{1}$ respectively.

For the rank-1 and rank-2 non-cooperation transmission mode, we can treat them as the conventional MIMO system. The MRC and MMSE receiver structures are adopted and derived in Section 4.2. Based on the corresponding receiver, we can demodulate the desired data for each RRH-user and macro-user.

CHAPTER 6

Numerical Results

6.1 MIMO in LTE-A Systems

Based on [22] and [34], we briefly introduce the simulation parameters of MIMO systems. Our simulation environment is the 3GPP Case 1 2D, where the center frequency (CF) is 2 GHz; the inter site distance (ISD) is 500 meters; both the downlink and uplink bandwidth are 10 MHz; the penetration loss is 20 dB, and the user speed is 3 km/hr. The cellular system consists of nineteen cell sites with hexagonal grid, and each cell is divided into three sectors. All 57 sectors use the same frequency band. Furthermore, the frequency division duplex (FDD) transmission mode is adopted, the channel model is urban-macro SCM with high spread [26], and the maximum retransmission times is three. We have listed our simulation parameters in Table 6.1.

First, let us compare the eigenmode codebook selection mechanism with the optimal codebook selection mechanism. The former is mentioned in Section 4.1, and the latter is simulated by testing all the possible codewords. Taking the 2×2 SU-MIMO system as example shown in Fig. 6.1, we find that the spectral efficiency of the eigen mode codebook selection mechanism is quite closed to that of the optimal codeobok selection mechanism. Thus, we can find a suitable codeword by using the eigen mode transmission rather than a exhaustive search.

Then, we compare the SU/MU-MIMO simulation results with existing results

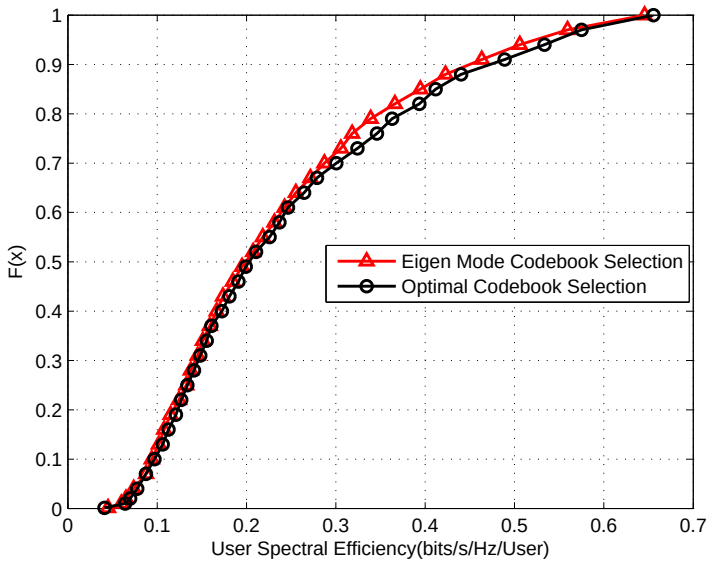

Figure 6.1: Spectral efficiency for 2x2 SU-MIMO with different codebook selection mechanisms.

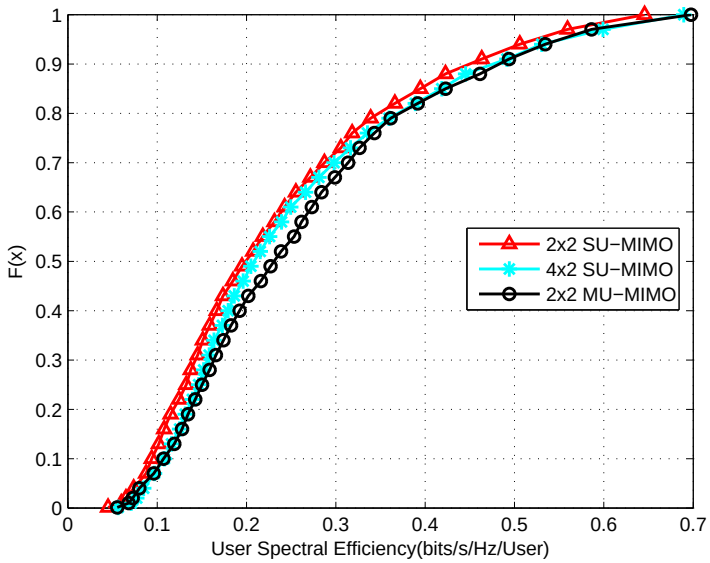

Figure 6.2: MIMO downlink normalized user throughput in LTE-A systems.

in 3GPP. The cumulative distribution function (CDF) figures for the SU/MU-MIMO user spectral efficiency are shown in Fig. 6.2. Based on [23] and [33], we list the maximum and minimum simulation results of other companies in Table 6.2, which shows the cell-average and cell-edge spectral efficiency of SU-MIMO and MU-MIMO systems. All of our results fall into the range of others in 3GPP. For example, in the 2×2 SU-MIMO system, the minimum and maximum values of the cell-average spectrum efficiency are 2.14 (bits/s/Hz) and 2.47 (bits/s/Hz) with our work obtaining a value of 2.37 (bits/s/Hz). In the 2×2 MU-MIMO system, the minimum and maximum values of the cell-average spectral efficiency are 2.56 (bits/s/Hz) and 2.77 (bits/s/Hz) with our work obtaining a value of 2.62 (bits/s/Hz).

6.2 Hierarchical Base Station Cooperation

In addition to the simulation parameters given in Table 6.1, other parameters for the **RRH nodes** are added [22]. The number of fixed RRH nodes per sector is 4; the number of transmit antennas in each RRH nodes is 2; the transmit power is 30 dBm; Omni-antennas are used; the pathloss model is $140.7 + 36.7\log_{10}(d)$, where d is in kilometers. The minimum distance between each user and each RRH node is 10 meters; the minimum distance between RRH nodes is 40 meters; the minimum distance between each RRH node and the corresponding macro-BS is 70 meters. We have listed additional parameters for the RRH nodes in Table 6.3. Note that proportional fair scheduling and rank adaptation techniques are also adopted in the simulation.

6.2.1 Cooperation with Single Cell ID

Spectral Efficiency

Based on the previous transmit signal model, receive algorithm, adaptive MCS, and ARQ mechanism, we show the numerical and simulation results from the spectral efficiency aspect in this section.

In intuition, more coordinated RRH nodes can yield larger spectral efficiency. It is reasonable in the single-cell case because more cooperative RRH nodes can enhance the magnitude of the receive signal. This phenomenon is illustrated in Fig. 6.3, where d is equal to $0.8R$, and the transmit power of macro-BS and each RRH node are 26 dBm and 10 dBm respectively. When considering the system in the single-cell case (no ICI), the 5% cell-edge spectral efficiency increases as the number of selected serving RRH nodes N_{HS} increases.

In multi-cell case, however, more coordinated RRH nodes will degrade the

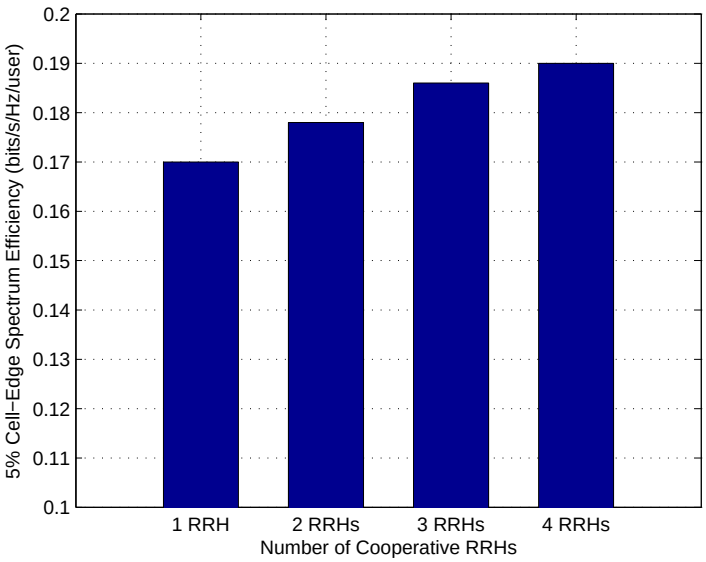

Figure 6.3: 5% cell-edge spectral efficiency of the HBSC-S systems without ICI.

spectral efficiency. Figure 6.4 shows the 5% cell-edge spectral efficiency and Fig. 6.5 shows the cell-average spectral efficiency, and the 2×2 SU-MIMO system is regarded as our baseline. We observe that when the number of selected serving RRH nodes N_{HS} increases, both the 5% cell-edge and cell-average spectral efficiency decreases significantly. This can be interpreted to indicate that an increase in N_{HS} results in an increase in the total inter-cell interference from all the RRH nodes. However, because of the small coverage of RRH nodes, the desired receive signal power does not increase significantly as N_{HS} increases. Taking $d = 0.7R$ as the example, the 5% cell-edge spectral efficiency is 0.1060 (bits/s/Hz/) with $N_{HS} = 1$, but only 0.0956 (bits/s/Hz/) and 0.0846 (bits/s/Hz/) with $N_{HS} = 3$ and $N_{HS} = 4$ respectively. The phenomenon is the same when considering the cell-average spectral efficiency. The cell-average spectral efficiency is is 2.8335 (bits/s/Hz/) with $N_{HS} = 1$, but only 2.6255 (bits/s/Hz/) and 2.5779 (bits/s/Hz/) with $N_{HS} = 3$ and $N_{HS} = 4$ respectively. When there are too many serving RRH nodes, the spectral efficiency deteriorates more than in the conventional SU-MIMO system.

Another observation is that different positions for the RRH nodes yield different performances. Taking $N_{HS} = 1$ as the example, the 5% cell-edge spectral efficiency is the highest (0.1048 bits/Hz/s) when $d = 0.7R$, and the cell-average spectral efficiency is the highest (2.8709 bits/Hz/s) when $d = 0.6R$. When the distance d is too small or too large, it results in a worse performance. This is because if d is too small, or equivalently, the RRH nodes are close to the macro-BS, the RRH nodes can not further help a majority of the users in the macro-cell. On the contrary, if d is too large, the RHH nodes in the other macro-cells cause very large inter-cell interference to the observing cell. Hence, it results in a worse performance.

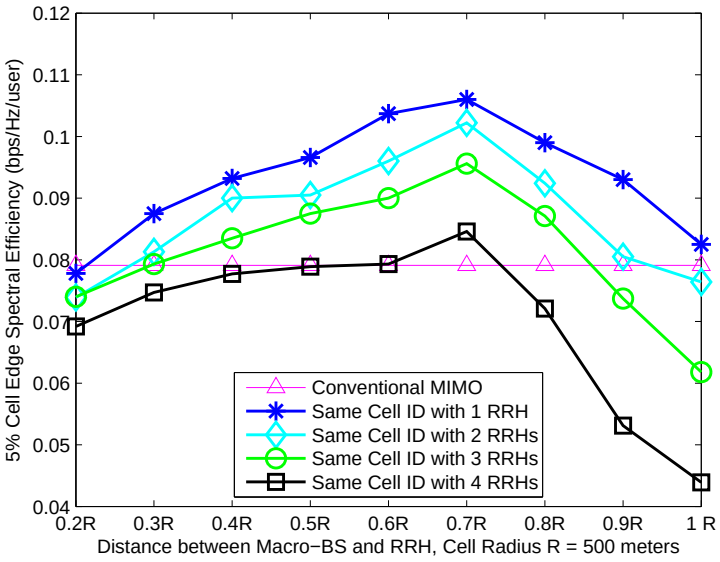

Figure 6.4: 5% cell-edge spectral efficiency of the HBSC-S systems.

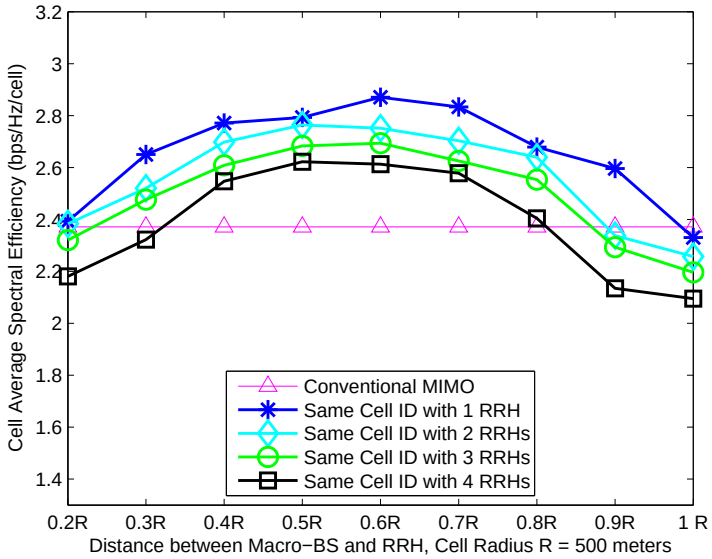

Figure 6.5: Cell-average spectral efficiency of the HBSC-S systems.

Energy Efficiency

We adopt the power consumption model mentioned in section 3.4. Since the RRH nodes share the same cell ID with the macro-BS, these nodes can be regarded as distributed antennas of the macro-BS. Thus, the RRH nodes are not required to perform MIMO and OFDM signal processing. The signal processing is performed at the macro-BS, and then the macro-BS delivers the same transmit data to each RRH node via the backhaul. Each RRH node only needs to transmit the data that comes from the macro-BS. Based on (3.17), we list the total system consumed power per sector in Table 6.4, where P_{bh} depends on the current transmit data rate.

Once we have the power model, we can derive the energy efficiency metric E_{total} in bits per Joule. The simulation results for the energy efficiency are shown in Fig. 6.6. Although the hierarchical network MIMO system consumes additional power (in the backhaul network and at RRH nodes) as compared to the SU-MIMO system, applying the HBSC-S system with fewer RRH nodes yields a more energy-efficient performance as well as better spectral efficiency. For example, with $d = 0.6R$ and $N_{HS} = 1$, the cell-average spectral efficiency is 2.8709 (bit/s/Hz), and the energy efficiency is 53170 (bits/Joule). However, in the conventional SU-MIMO system, the cell-average spectral efficiency is only 2.3715 (bit/s/Hz), and the energy efficiency is only 46205 (bits/Joule). The HBSC-S system outperforms the conventional SU-MIMO in terms of both the spectral efficiency and the energy efficiency with the proper d and N_{HS}.

6.2.2 Cooperation with Multiple Cell IDs

Spectral Efficiency

We shows the spectral efficiency of the HBSC-M system here. In Figs. 6.4 and 6.5, we compare the HBSC-M system with both the HBSC-S system and the SU-MIMO

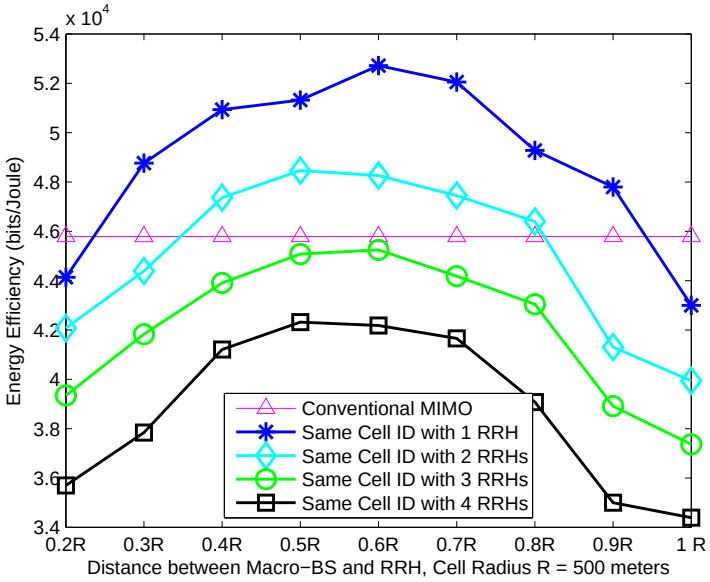

Figure 6.6: Energy efficiency of the the HBSC-S systems.

system. It can be seen that the HBSC-D system yields better cell-edge and cell-average spectral efficiency. This is because the HBSC-M system can serve multiple users simultaneously and suppress the intra-cell interference. It exploits more degrees of freedom in the spatial domain.

Different positions of the RRH node also yield different performance. This phenomenon is the same as that in the HBSC-S systems. For example, the 5% cell-edge spectral efficiency is the highest (0.1159 bits/Hz/s) when $d = 0.6R$, and the cell-average spectral efficiency is the highest (3.4421 bits/Hz/s) when $d = 0.7R$. If the distance d is too small or too large, it results in a worse performance. The reasons are similar with the HBSC-S systems. If d is too small, or equivalently, RRH nodes are close to the macro-BS, the RRH nodes can not further help a majority of the users in the macro-cell. If d is too large, the spectral efficiency of the cell-edge user in the HBSC-M system deteriorates more than in the HBSC-S systems. The reason is that if the user locate at the edge of the cell, it is better for the RRH node utilizing all transmit power to serve the cell-edge user. However, in the HBSC-M system, the RRH nodes need to serve another co-scheduled user in the mean time. The cell-edge user get only about half receive power compared to the HBSC-S systems (another help from the macro-BS is slight due to the large distance from the macro-BS to the user), but much interference from the other macro-cells interferes the users if d is too large. Hence, the cell-edge users in the HBSC-M system have less spectral efficiency than those in the HBSC-S systems with $d \geq 0.8R$.

Energy Efficiency

The power consumption model in Section 3.4 is adopted. Because the RRH nodes have different cell IDs with the macro-BS, these nodes need to serve their own users or jointly serve both RRH-user and macro-user. Hence, both macro-BS and each RRH node are required to perform the signal processing. Furthermore, the data

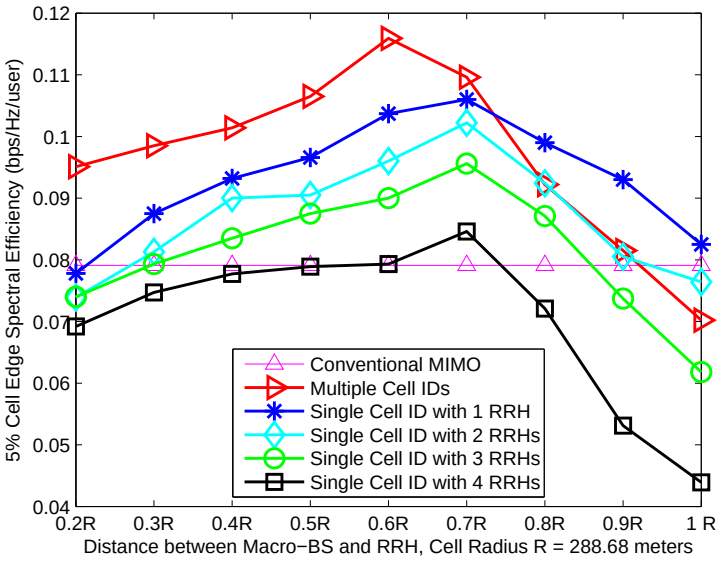

Figure 6.7: 5% cell-edge spectral efficiency of the HBSC-M systems.

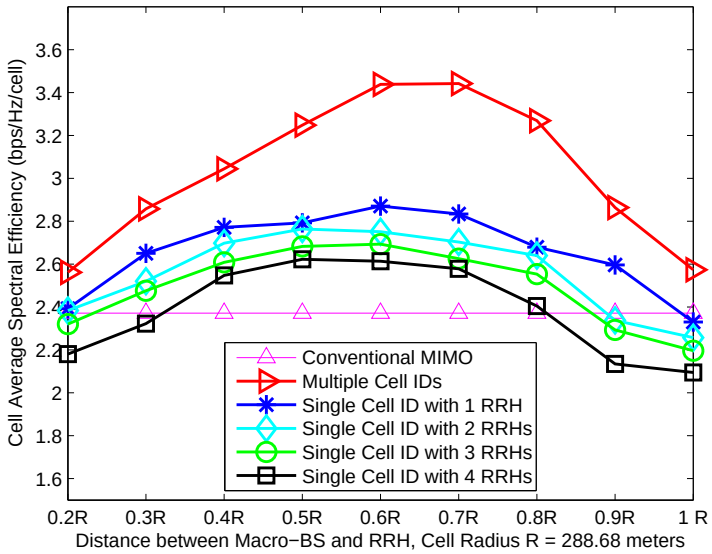

Figure 6.8: Cell-average spectral efficiency of the HBSC-M systems.

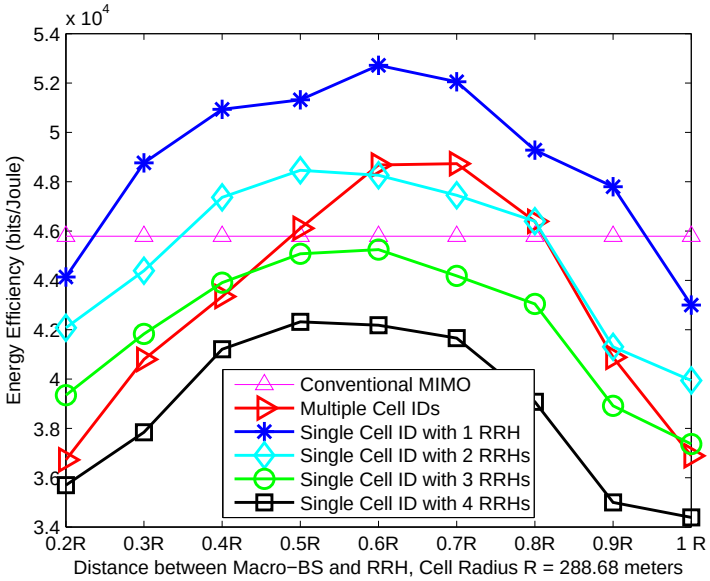

Figure 6.9: Energy efficiency of the HBSC-M systems.

are exchanged in the whole coordinated network. Namely, each RRH node needs to transmit the data for the RRH-user to the macro-BS via the backhaul, and vice versa. Hence, the consumed power of transmitting the data via the backhaul P_{bh} is considered in both the macro-BS and RRH nodes. Based on (3.17), we list the total system consumed power per sector in Table 6.5, where P_{bh} depends on the current transmit data rate.

Once we have the power model, we can derive the energy efficiency metric E_{total} in bits per Joule. The simulation results are shown in Fig. 6.9. It comes out a interesting result that although the HBSC-M system outperforms the HBSC-S system in spectral efficiency, the power consumption is not efficient for the HBSC-M system. For example, with $d = 0.6R$ and $N_{HS} = 1$, the cell-average energy efficiency is 53170 (bits/Joule) in the HBSC-S system, but only 48997 (bits/Joule) in the HBSC-M system. Taking $d = 0.6R$ shown in Fig. 6.10, we find out that if the HBSC-S systems

are adopted, both the spectral efficiency and energy efficiency increase when using less RRH nodes. However, if we adopt the HBSC-M system, the spectral efficiency increases but the energy efficiency decreases compared to the HBSC-S system with $N_{HS} = 1$. There is a tradeoff between the spectral efficiency and the energy efficiency. We can obtain a better spectral efficiency but a worse energy efficiency by applying the HBSC-M system. Table 6.6 shows the detailed energy efficiency and spectral efficiency gain by regarding the conventional MIMO system as the baseline. We obtain a better spectral efficiency (45% gain) by applying the CoMP-M system but obtain a better energy efficiency (15% gain) by applying the CoMP-S system.

We also evaluate the minimum consumed power at BSs that aim to achieve the target spectral efficiency 2.40 ($bits/s/Hz$) required by ITU. As shown in Fig. 6.11, the conventional MIMO system consumes about 524 (W) per sector and the HBSC-M system consumes about 492 (W) per sector to achieve the spectral efficiency requirement, however, the HBSC-S system with one cooperated RRH node consumes only 455 (W) per sector. The HBSC-S system saves about 13 % power consumption compared to the conventional MIMO systems.

6.3 Summary

In this chapter, we introduced the simulation methodology for SU/MU-MIMO systems and evaluated the MIMO systems in the LTE-A environment. Our simulation results are consistent with the existing results in 3GPP.

Moreover, we demonstrated both the spectral efficiency and the energy efficiency in two kinds of HBSC systems:

(1) RRH nodes share the same cell ID with the corresponding macro-BS.

(2) Each RRH node has the individual cell IDs different from the corresponding macro-

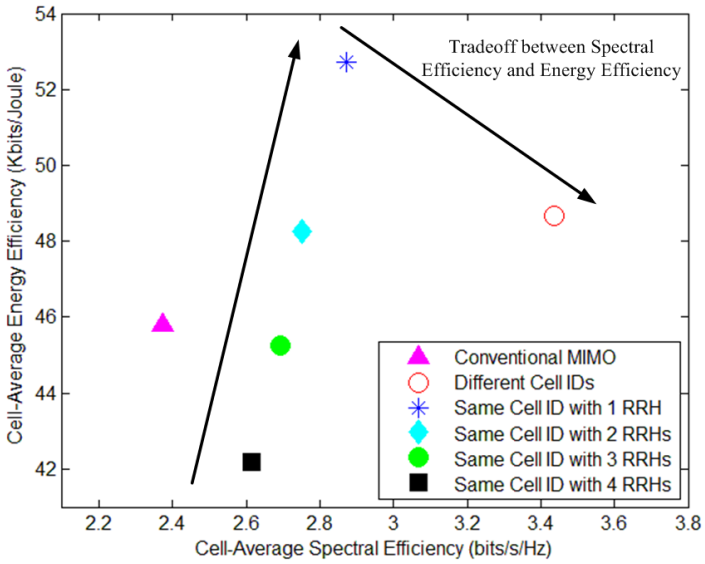

Figure 6.10: Comparison between energy efficiency and spectral efficiency , $d = 0.6R$.

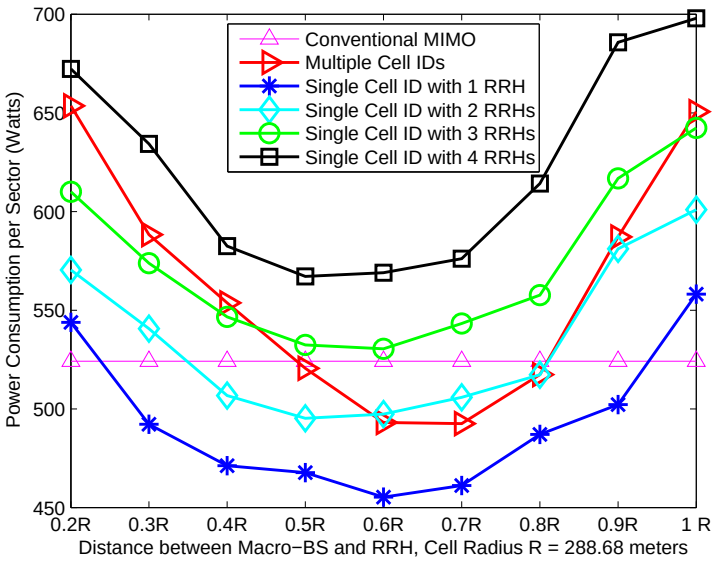

Figure 6.11: Power consumption per sector of HBSC systems for targeting at 2.40 bits/s/Hz.

BS.

In (1), the HBSC-S systems outperforms the SU-MIMO system in terms of both the spectral efficiency and the energy efficiency. Furthermore, we find that too many RHH nodes may yield a worse performance, and that the best position for each RRH node is $d = 0.6R \sim 0.7R$. In (2), we find out that there is a tradeoff between the spectral efficiency and the energy efficiency. By applying the HBSC-M system, we can obtain better spectral efficiency but lose some energy efficiency compared to the HBSC-S systems. Further, the best position of each RRH node is still $d = 0.6R \sim 0.7R$ in the HBSC-M systems.

Table 6.1: **Simulation Parameters for MIMO systems**

Parameter	**Value**
Duplex Method	FDD
DL Transmission Scheme	OFDMA
Subcarrier Number	600
Downlink Transmit Antenna Number	2 and 4
Downlink Receive Antenna Number	2
ISD	500 meters
Macro-cell Number	19
Number of Users per Sector	10
User Speed	3 km/hr
Network Synchronization	synchronization
Downlink Scheduler	proportional fair scheduling in time and frequency
Downlink ARQ	a maximum of four transmission times
Downlink Receiver Type	MMSE
BS Transmit Power	46 dBm
Noise Power Density	-174 dBm/Hz
Antenna Configuration at Receiver	0.5 wavelength separation
Antenna Configuration at Transmitter	10 wavelength separation
Minimum Distance between user and macro-cell	35 meters
Channel Model	SCM urban macro
Antenna Pattern	$A_H(\phi) = -\min\left[12\left(\frac{\phi}{\phi_{3dB}}\right), A_m\right]$ $\phi_{3dB} = 70°, A_m = 25dB$
Penetration Loss	20 dB
Pathloss Model	$128.1 + 37.6log_{10}(d)$, d in km
Shadowing Model	lognormal with zero mean and 8 dB standard deviation

Table 6.2: **Performance Evaluation Comparison**

	Min-value of other companies (bits/s/Hz)	**Our Work** (bits/s/Hz)	**Max**-value of other companies (bits/s/Hz)
2×2 SU-MIMO Downlink Cell-Average Spectral Efficiency	2.14	**2.37**	2.47
2×2 SU-MIMO Downlink 5% Cell-Edge Spectral Efficiency	0.072	**0.079**	0.100
4×2 SU-MIMO Downlink Cell-Average Spectral Efficiency	2.34	**2.52**	2.66
4×2 SU-MIMO Downlink 5% Cell-Edge Spectral Efficiency	0.085	**0.089**	0.110
2×2 MU-MIMO Downlink Cell-Average Spectral Efficiency	2.56	**2.62**	2.77
2×2 MU-MIMO Downlink 5% Cell-Edge Spectral Efficiency	0.070	**0.086**	0.110

Table 6.3: **Simulation Parameters for RRH Nodes**

Parameter	**Value**
RRH nodes number per sector	4
Downlink RRH nodes Transmit Antenna Number	2
RRH Transmit Power	30 dBm
Antenna Configuration at RRH nodes	10 wavelength separation
Antenna Pattern	Omni-antennas
Pathloss Model	$140.7 + 36.7log_{10}(d)$, d in km
Minimum Distance between user and RRH nodes	10 meters
Minimum Distance between each RRH node	40 meters
Minimum Distance between Macro base station and RRH nodes	75 meters

Table 6.4: **Total System Consumed Power per Sector in HBSC-S Systems**

Systems	$N_{HS} = 1$
Macro-BS Consumed Power (Watts)	$461.93 + 1 \times P_{bh}$
RRH nodes Consumed Power (Watts)	1×11.1
Total System Consumed Power (Watts)	$473.03 + 1 \times P_{bh}$
Systems	$N_{HS} = 2$
Macro-BS Consumed Power (Watts)	$461.93 + 2 \times P_{bh}$
RRH nodes Consumed Power (Watts)	22.2
Total System Consumed Power (Watts)	$484.13 + 2 \times P_{bh}$
Systems	$N_{HS} = 3$
Macro-BS Consumed Power (Watts)	$461.93 + 3 \times P_{bh}$
RRH nodes Consumed Power (Watts)	33.3
Total System Consumed Power (Watts)	$495.23 + 3 \times P_{bh}$
Systems	$N_{HS} = 4$
Macro-BS Consumed Power (Watts)	$461.93 + 4 \times P_{bh}$
RRH nodes Consumed Power (Watts)	44.4
Total System Consumed Power (Watts)	$506.33 + 4 \times P_{bh}$

Table 6.5: **Total System Consumed Power per Sector in HBSC-M Systems**

Systems	
Macro-BS Consumed Power (Watts)	$461.93 + P_{bh}$
RRH nodes Consumed Power (Watts)	$138.6 + P_{bh}$
Total System Consumed Power (Watts)	$600.53 + 2 \times P_{bh}$

Table 6.6: **Comparison between Energy Efficiency and Spectral Efficiency ($\mathbf{d = 0.6R}$)**

	Spectral Efficiency Gain	Energy Efficiency Gain
HBSC-M	**45**%	6%
HBSC-S with $N_{HS} = 1$	21%	**15**%
HBSC-S with $N_{HS} = 2$	16%	5%
HBSC-S with $N_{HS} = 3$	14%	−1%
HBSC-S with $N_{HS} = 4$	10%	−8%
Conventional MIMO	0%	0%

CHAPTER 7

Conclusions and Future Research

7.1 Conclusions

We discussed the simulation methodology of SU/MU-MIMO systems in the 3GPP LTE-A environment, and gave a simulation flow chart. Both the cell-average and the cell-edge spectral efficiency are consistent with other existing results from the partners in 3GPP .

Based on the SU/MU simulator, we extended it to the hierarchical base station cooperation system, which is divided into two categories

(1) RRH nodes share the same cell ID with the corresponding macro-BS.

(2) Each RRH node has an individual cell ID that is different from the corresponding macro-BS.

Furthermore, two metrics, i.e. the spectral efficiency and the energy efficiency, were considered in our thesis.

For the HBSC-S system, it outperforms the SU-MIMO system in terms of both the spectral efficiency and the energy efficiency. However, too many RRH nodes may yield a worse performance in the multi-cell environment, since the RRH nodes from the other macro-cell cause much interference. Moreover, various distances between the RRH node and the macro-BS result in different performances. Generally, the distances are the best from $0.6R$ to $0.7R$, where R is the cell radius.

For the HBSC-M system, the spectral efficiency is further enhanced compared to the the HBSC-S system. However, we found out that there are tradeoffs between the spectral efficiency and the energy efficiency. Compared to the conventional MIMO systems, we obtain a better spectral efficiency (45% gain) by applying the CoMP-M system but obtain a better energy efficiency (15% gain) by applying the CoMP-S system.

7.2 Future Research

By fixing some RRH nodes in the HBSC systems, we can enhance the receive signal quality of the cell-edge users and improve the cell-edge spectral efficiency. However, the fixed RRH nodes cause the extra interference to other cells since we do not co-operate the neighboring macro-cells. If we jointly consider the cooperation at both the intra-cell and the inter-cell level with adaptive cooperation schemes, the interference problem caused by the RRH nodes can be further mitigated, and we can further enhance the cell-edge spectral efficiency.

Besides, the spectral efficiency is not the only metric we should consider. There must be some tradeoffs between the spectral efficiency and the energy efficiency. In the green communication networks, how to strike a balance between these two metrics is crucial.

Bibliography

[1] I. E. Telatar, "Capacity of multi-antenna gaussian channels," *European Transactions on Telecommunications*, vol. 10, no. 6, pp. 585–595, Dec. 1999.

[2] S. Shamai and B. M. Zaidel, "Enhancing the cellular downlink capacity via co-processing at the transmitting end," *IEEE Vehicular Technology Conference Spring*, vol. 3, pp. 1745 – 1749, May 2001.

[3] H. Zhang and H. Dai, "Cochannel interference mitigation and cooperative processing in downlink multicell multiuser MIMO networks," *EURASIP Journal on Wireless Communications and Networking*, vol. 2004, no. 2, pp. 222–235, 2004.

[4] G. J. Foschini, K. Karakayali, and R. A. Valenzuela, "Coordinating multiple antenna cellular networks to achieve enormous spectral efficiency," *IEE Proceedings-Communications*, vol. 153, no. 4, pp. 548 – 555, Aug. 2006.

[5] S. Jing, D. N. C. Tse, J. B. Soriaga, J. Hou, J. E. Smee, and R. Padovani, "Multicell downlink capacity with coordinated processing," *EURASIP Journal on Wireless Communications and Networking*, vol. 2008, 2008.

[6] H. Huang, M. Trivellato, A. Hottinen, M. Shafi, P. Smith, and R. Valenzuela, "Increasing downlink cellular throughput with limited network MIMO coordination," *IEEE Transactions on Wireless Communications*, vol. 8, no. 6, Jun. 2009.

[7] N. Kusashima, I. D. Garcia, K. Sakaguchi, K. Araki, S.Kaneko, and Y. Kishi, "Fractional base station cooperation cellular network," *International Conference on Information, Communications and Signal Processing*, pp. 1–5, Dec. 2009.

[8] L. C. Wang and C. J. Yeh, "A three-cell coordinated network MIMO with fractional frequency reuse and directional antennas," *IEEE International Conference of Communications*, May 2010.

[9] *IEEE. Standard 802.16. Part 16: air interface for fixed and mobile broadband wireless access systems – DRAFT amendment to IEEE standard for local and metropolitan area networks – advanced air interface*, IEEE P802.16m/D4, Feb. 2010.

[10] H. Dahrouj and W. Yu, "Coordinated beamforming for the multicell multi-antenna wireless system," *IEEE Transactions on Wireless Communications*, vol. 9, no. 5, May 2010.

[11] U. Jang, K. Lee, K. Cho, and W. Ryu, "Transmit beamforming based inter-cell interference alignment and user selection with CoMP," *IEEE Vehicular Technology Conference Fall*, pp. 1–5, 2010.

[12] Q. Li, Y. Yang, S.Fang, and G. Wu, "Coordinated beamforming in downlink CoMP transmission system," *International ICST Conference on Communications and Networking*, 2010.

[13] X. Xia, G. Wu, S. Fang, Y. Tian, and S. Li, "Coordinatd scheduling and precoding in multicell MIMO system," *Pacific-Asia Conference on Circuits, Communications and System*, pp. 387–389, 2010.

[14] 3GPP, R1-101646, "Performance evaluation of intra-site DL CoMP," Ericsson, ST-Ericsson, Feb. 22 - 26, 2010.

[15] F. Richter, A. J. Fehske, and G. Fettweis, "Energy efficiency aspects of base station deployment strategies for cellular networks," *IEEE Vehicular Technology Conference Fall*, Sep. 2009.

[16] A. J. Fehske, P. Marsch, and G. P. Fettweis, "Bit per Joule efficiency of cooperating base stations in cellular networks," *IEEE GLOBECOM Workshops*, Dec. 2010.

[17] 3GPP, TR 36.913 v9.0.0, "Requirements for further advancements for evolved universal terrestrial radio access (E-UTRA)," Dec. 2009.

[18] 3GPP, TS 36.211 v9.1.0, "Evolved universal terrestrial radio access (E-UTRA) physical channels and modulation," Mar. 2010.

[19] J. C. Ikuno, M. Wrulich, and M. Rupp, "System level simulation of LTE networks," *IEEE Vehicular Technology Conference Spring*, May 2010.

[20] G. Piro, L. A. Grieco, G. Boggia, F. Capozzi, and P. Camarda, "Simulating LTE cellular systems : an open-source framework,," *IEEE Transaction on Vehicular Technology*, vol. 60, no. 2, Feb. 2011.

[21] 3GPP, R1-092742, "Email discussion summary on calibration step 1c," Ericsson, Jun. 29 - July 3, 2009.

[22] 3GPP, TR 36.814 v9.0.0, "Evolved universal terrestrial radio access (E-UTRA); further advancements for E-UTRA physical layer aspects," Mar. 2010.

[23] 3GPP, R1-100823, "Summary of evaluation results for 3GPP requirements," NTT DOCOMO, Jan. 18-22, 2010.

[24] Y. J. Liu, T. T. Chiang, and L. C. Wang, "Physical layer performance calibration for 3GPP LTE-A systems," *accepted in IEEE Asia Pacific Wireless Communication Symposium*, 2011.

[25] 3GPP, TR 36.996 v9.0.0, "Spatial channel model for Multiple Input Multiple Output (MIMO) simulations," Dec. 2009.

[26] J. Salo, G. Del Galdo, J. Salmi, P. Kyosti, M. Milojevic, D. Laselva, and C. Schneider. (2005, Jan.) MATLAB implementation of the 3GPP Spatial Channel Model (3GPP TR 25.996). [Online]. Available: http://www.tkk.fi/Units/Radio/scm/

[27] 3GPP, R1-111125, "CoMP simulation assumptions," NTT DOCOMO, Feb. 21 - 25, 2011.

[28] 3GPP, R1-110867, "CoMP with lower Tx power RRH in heterogeneous network," NTT DOCOMO, Feb. 21-25, 2011.

[29] O. Arnold, F. Richter, G. P. Fettweis, and O. Blume, "Power consumption modeling of different base station types in heterogeneous cellular networks," *Future Network and Mobile Summit*, Jun. 2010.

[30] A. J. Fehske, F. Richter, and G. P. Fettweis, "Energy efficiency improvements through micro sites in cellular mobile radio networks," *IEEE GLOBECOM Workshops*, Dec. 2009.

[31] H. M. Kwon and T. G. Birdsall, "Channel capacity in bits per joule," *IEEE Journal of Oceanic Engineering*, vol. 11, no. 1, Jan. 1986.

[32] E. V. Belmega and S. Lasaulce, "Energy-efficient precoding for multiple-antenna terminals," *IEEE Transactions on Signal Processing*, vol. 59, no. 1, Jan. 2011.

[33] 3GPP, TS 36.213 v9.3.0, "Evolved universal terrestrial radio access (E-UTRA) physical layer procedures," Sep. 2010.

[34] 3GPP, TR 25.814 v7.1.0, "Physical layer aspects for evolved universal terrestrial radio access (E-UTRA)," Sep. 2006.

[35] F. Boccardi and H. Huang, "A near-optimum technique using linear precoding for the MIMO broadcast channel," *IEEE International Conference on Acoustics, Speech and Signal Processing*, vol. 3, pp. 17–20, 2007.

[36] L. Thiele, T. Wirth, M. Schellmann, Y. Hadisusanto, and V. Jungnickel, "MU-MIMO with localized downlink base station cooperation and downtilted antennas," *IEEE International Conference on Communications Workshops*, pp. 1–5, 2009.

[37] N. Jindal, "Antenna combining for the MIMO downlink channel," *IEEE Transactions on Wireless Communications*, vol. 7, no. 10, pp. 3834–3844, Oct. 2008.

[38] S. Fang, G. Wu, Y. Xiao, and S. Q. Li, "Multi-user MIMO linear precoding with grassmannian codebook," *WRI International Conference on Communications and Mobile Computing*, vol. 1, pp. 250–255, 2009.

[39] 3GPP, R1-110586, "Proposal for UE receiver assumption in CoMP simulations," LG Electronics, Motorola Mobility, Intel, Marvell, Samsung, ETRI, Orange, Renesas and Huawei, Jan. 17-21, 2011.

[40] J. Zhu, J. Liu, X. She, and L. Chen, "Investigation on precoding techniques in E-UTRA and proposed adaptive precoding scheme for MIMO systems," *Asia-Pacific Conference on Communications*, 2008.

[41] R. W. Heath and A. J. Paulraj, "Switching between diversiy and multiplexing in MIMO systems," *IEEE Transactions on Communications*, vol. 53, no. 6, Jun. 2005.

[42] 3GPP, R1-092646, "Dynamic SU/MU mode switching and rank adaptation," Motorola, Jun. 29 - Jul.3, 2009.

[43] 3GPP, R1-092739, "LTE Rel8/10 performance and IMT-Advanced requirements," Ericsson, ST-Ericsson, Jun. 29 - Jul.3, 2009.

[44] 3GPP, R1-092681, "LTE and LTE-Advanced performance," Samsung, Jun. 29 - Jul.3, 2009.

[45] L. Thiele, V. Jungnickel, M. Schellmann, and W. Zirwas, "Capacity scaling of multi-user MIMO with limited feedback in a multi-cell environment," *Conference Record of the Forty-First Asilomar Conference on Signals, Systems and Computers*, pp. 93–100, 2007.

[46] 3GPP, R1-094278, "Considerations on downlink MU-MIMO," ZTE, Oct 12 - 16, 2009.

[47] 3GPP, R1-111290, "CoMP phase 1 evaluation results," Motorola, May 9 - 13, 2011.

[48] 3GPP, R1-100902, "Considerations on interference coordination in Het-Net," CATT, Feb. 22-26, 2010.

[49] 3GPP, R1-100236, "Considerations on interference coordination in heterogeneous networks," LG Electronics, Jan. 18-22, 2010.

Vita

Tsung-Ting Chiang

He was born in Taiwan, R. O. C. in 1987. He received his B.S. at the Department of Communication Engineering, National Chiao-Tung University in 2009. From July 2009 to August 2011, he worked his Master degree in the Mobile Communications and Cloud Computing Lab at the Institute of Communication Engineering at National Chiao-Tung University. His research interests are in the field of wireless communications.